Precipitation Scenarios over Iberia: A Comparison between Direct GCM Output and Different Downscaling Techniques

RICARDO M. TRIGO

Department of Physics, Faculty of Sciences, University of Lisbon, Lisbon, Portugal, and Climatic Research Unit, University of East Anglia, Norwich, United Kingdom

JEAN P. PALUTIKOF

Climate Research Unit, University of East Anglia, Norwich, United Kingdom

(Manuscript received 16 January 2001, in final form 7 June 2001)

ABSTRACT

The Iberian rainfall regime is characterized by a strong seasonal cycle and large interannual variability. Typically, frequency distributions of monthly precipitation present a large spread of values, implying frequent episodes of very wet or very dry years. Unfortunately, the most recent generation of general circulation models (GCMs) still has serious problems when modeling monthly precipitation over southern Europe. However, these models are able to reproduce the main patterns of atmospheric circulation, such as those derived from a principal component analysis of the sea level pressure anomaly field. Many downscaling techniques have been developed in recent years, all having in common the need to establish statistical links between the large-scale circulation and the observed precipitation at a local or regional scale. The final objective is usually the application of such transfer functions to GCM output.

In this work, linear and nonlinear downscaling transfer functions are developed based on artificial neural networks (ANNs), to downscale monthly precipitation to nine grid boxes over the Iberian Peninsula. The nonlinear ANN models were run 20 times, with different initial conditions, in order to study the stability of the final results. All the models were developed on a seasonal basis, calibrated between 1901 and 1940 and validated between 1941 and 1990. It was found that linear or slightly nonlinear ANN models (with just one node in the first layer) were more capable of reproducing the observed precipitation than more complex nonlinear ANN models. GCM data from a greenhouse gas–plus-sulfates run from the Hadley Centre Model (HadCM2) were used to reproduce present-day precipitation over Iberia. It was found that the precipitation characteristics (mean, variance, and empirical distribution) were better reproduced by the downscaled results than by the GCM direct output. Precipitation scenarios constructed for the future (2041–90) reveal an increase of precipitation in winter and small decreases in most sectors of Iberia for the spring and autumn seasons. Such scenarios are in good agreement with those obtained by other researchers using different downscaling techniques with HadCM2 data.

1. Introduction

The Iberian Peninsula precipitation regime is characterized by high variability in both the spatial and temporal domains. The study of precipitation variability is therefore of primary relevance, mainly because of its impact on society, on economic activities such as agricultural production, and on land use and water resources. The distribution of orography (Fig. 1) and the Atlantic origin of many synoptic disturbances contributes to enormous spatial variations in the amounts of observed precipitation (Serrano et al. 1999). Annual precipitation values over Iberia range from 300 mm yr^{-1} in the coastal semidesertic southeast regions (Romero et al. 1998) to more than 1200 mm yr^{-1} in the northwestern provinces (Rodriguez-Puebla et al. 1998). The spatial distribution of Iberian precipitation, as well as its seasonal variability, may be explained to a large extent in terms of the broad characteristics of the global circulation (e.g., seasonal movements of the Azores high pressure system) in the context of the regional geography (e.g., latitude, orography, oceanic and continental influences). However, such a simplistic framework cannot explain interannual variability, that is, the large range of values of precipitation observed from year to year. Previous studies have shown that interannual variability is mainly due to the corresponding interannual variability of the main large-scale atmospheric circulation modes affecting Iberia (von Storch et al. 1993; Rodriguez-Puebla et al. 1998). In particular, several authors have used a variety of statistical techniques to

Corresponding author address: Ricardo Machado Trigo, Grupo de Meteorologia, Departamento de Física, Faculdade de Ciências, Universidade de Lisboa, Campo Grande Ed C8, Piso 6, 1749-016 Lisbon, Portugal.
E-mail: rtrigo@fc.ul.pt

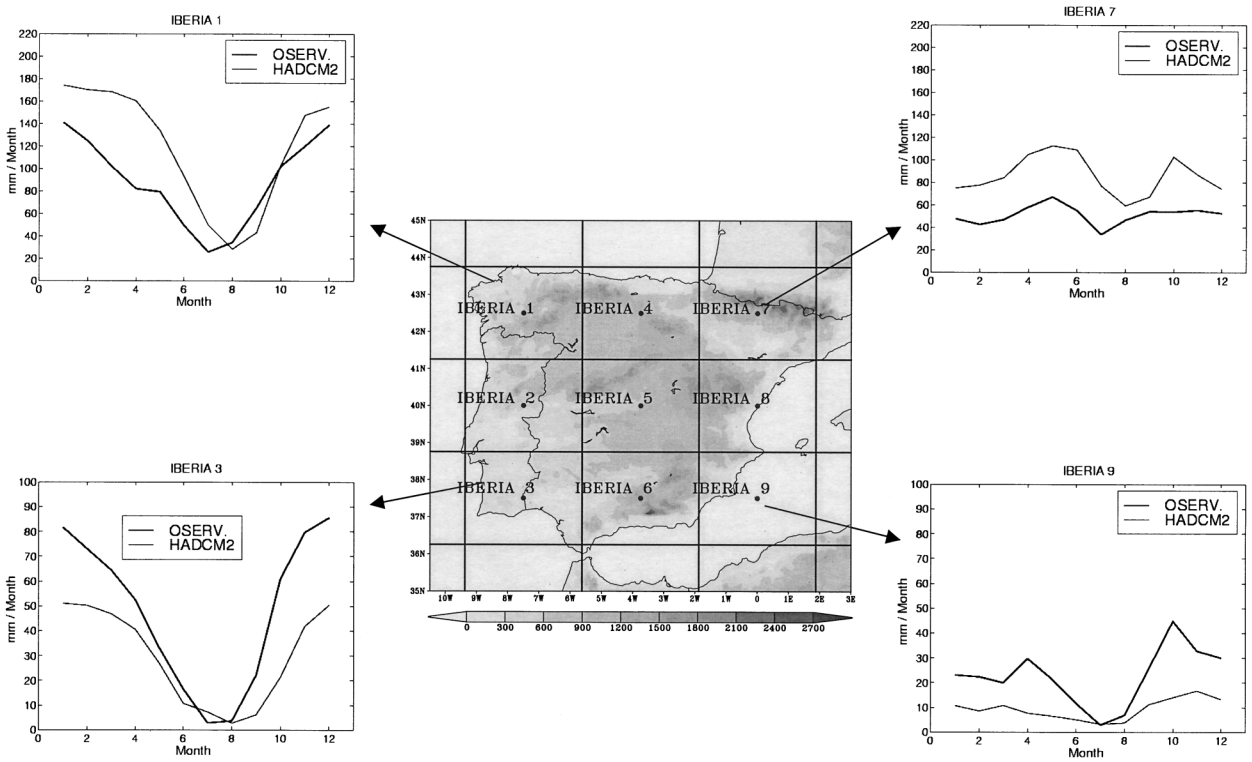

FIG. 1. The nine grid boxes defined over Iberia. The topography of the Iberian Peninsula is represented, darker gray corresponding to higher elevations. The seasonal cycle of observed and present-day HadCM2 GS precipitation for four grid boxes is also shown. (Note the different vertical scales for Iberia 1 and 7 as compared with Iberia 3 and 9.)

establish quantitative relationships between the Iberian monthly precipitation and the North Atlantic oscillation (Hurrel 1995; Rodó et al. 1997; Rocha 1999; Ulbrich et al. 1999; Goodess and Jones 2001, hereinafter GJ) or the Southern Oscillation (Laita and Grimalt 1997; Rodó et al. 1997; Rodriguez-Puebla et al. 1998; Rocha 1999). However, other features at the synoptic and smaller scales play an important role in terms of daily local precipitation regimes. Recently, a number of automated classifications of daily synoptic circulation patterns affecting Portugal and Spain have been developed to study their impact on daily precipitation (Zhang et al. 1997; Corte-Real et al. 1998, 1999; Goodess and Palutikof 1998; Trigo and DaCamara 2000; GJ).

The large east–west and north–south precipitation gradients coupled with strong seasonal and interannual variability make Iberia one of the most challenging regions of Europe to study in terms of climate change

TABLE 1. Summary of major applications of downscaling techniques over the Iberian region. Legend for techniques is PCA: Principal Component Analysis; CCA: Canonical Correlation Analysis; MARS: Multiple Adaptive Regression Splines; SSA: Singular Spectrum Analysis; CWT: Circulation Weather Types; ANNs: Artificial Neural Networks.

	Studied variable	Main techniques employed to classify large-scale circulation	GCM
Von Storch et al. (1993)	Winter Iberian precipitation	PCA coupled with CCA	ECHAM1
Corte-Real et al. (1995)	Monthly winter precipitation over Portugal	PCA coupled with MARS	UKTR
Cubasch et al. (1996)	Daily winter precipitation over Spain	PCA coupled with analogs	ECHAM1
Goodess and Palutikof (1998)	Daily precipitation in southern Spain	Circulation weather types and weather generator	UKTR
Corte-Real et al. (1999)	Daily precipitation over Portugal	Cluster analysis coupled with PCA	HadCM2
Zorita and von Storch (1999)	Daily and monthly precipitation over Spain	PCA coupled with CCA and with analogs, ANNs	ECHAM3
Gonzalez-Rouco et al. (2000)	Winter Iberian precipitation	PCA coupled with CCA	HadCM2
Trigo and Palutikof (1999)	Daily Tmax and Tmin over Portugal	Circulation indices and ANNs	HadCM2

TABLE 2. Means and std devs of seasonal precipitation for all nine grid boxes, computed from observations and GCM data (values in parentheses) for 1941–90. Significant differences at the 5% level are highlighted with *.

	Winter		Spring		Autumn	
	Mean	Std dev	Mean	Std dev	Mean	Std dev
Iberia 1	136 (166)*	88 (82)	88 (154)*	51 (68)*	95 (98)	64 (65)
Iberia 2	102 (103)	69 (74)	70 (83)*	42 (56)*	71 (44)*	56 (46)*
Iberia 3	81 (51)*	57 (47)*	50 (38)*	35 (33)	54 (23)*	52 (29)*
Iberia 4	70 (71)	34 (34)	64 (77)*	28 (26)	69 (52)*	37 (29)*
Iberia 5	43 (91)*	32 (56)*	45 (89)*	26 (43)*	41 (62)*	29 (38)*
Iberia 6	67 (62)	53 (49)	50 (60)*	36 (40)	47 (47)	43 (39)
Iberia 7	48 (76)*	26 (31)*	57 (101)*	30 (37)*	54 (86)*	31 (51)*
Iberia 8	36 (29)*	30 (24)*	38 (37)	30 (26)	60 (39)*	50 (40)*
Iberia 9	25 (11)*	21 (11)*	24 (8)*	20 (10)*	35 (14)*	31 (15)*

scenarios. Despite an increasing ability to successfully model present-day climate, the latest generation of GCMs still has serious difficulties when modeling monthly/seasonal precipitation over Europe in general, and the Iberian Peninsula in particular (Cubasch et al. 1996; Christensen et al. 1997; Osborn and Hulme 1998). This situation is partly due to the poor spatial definition and the corresponding crude representation of the orography in GCMs. Even in Limited-Area Models (LAMs) it is not possible to properly deal with subgrid phenomena such as cloud formation and precipitation processes (Christensen et al. 1997).

On the other hand, GCMs are usually more successful at reproducing the main modes of sea level pressure (SLP) variability over the Atlantic/Europe region (Corte-Real et al. 1995; Osborn et al. 1999). This capacity has led some researchers to develop techniques to establish statistical links between the observed large-scale circulation and the precipitation at local stations (downscaling methods) and then to apply the derived transfer functions to GCM output. In particular, different authors have considered the possibility of downscaling precipitation over Iberia both on monthly (von Storch et al. 1993; Corte-Real et al. 1995) and daily (Cubasch et al. 1996; Goodess and Palutikof 1998; Corte-Real et al. 1999) timescales. A summary of recent downscaling applications developed for different winter Iberian climatic variables can be found in Table 1.

In recent years, a number of authors have adopted artificial neural networks (ANNs) as a tool to downscale from the large-scale atmospheric circulation to local or regional climate variables (Hewitson and Crane 1996: Cavazos 1997, 1999; Wilby and Wigley 1997; Crane and Hewitson 1998; Cavazos and Hewitson 2000, manuscript submitted to *J. Climate*). Some applications were developed with the specific purpose of constructing climate change scenarios (Hewitson and Crane 1996; Wilby and Wigley 1997; Crane and Hewitson 1998). In particular, the advantage of using ANNs to downscale daily values of maximum and minimum temperature over Portugal, for the purpose of constructing climate change scenarios, was demonstrated in a previous work (Trigo and Palutikof 1999, hereinafter TP99).

In order to evaluate the improvements that any downscaling technique can achieve when reproducing present-day climate, it is necessary to compare their results with those obtained from the corresponding GCM direct output. However, for precipitation these comparisons can be problematic due to the very nature of the precipitation output of a GCM. Many downscaling papers present an enormous discrepancy between the large number of observational stations needed to fully characterize the precipitation climatology of a region and the small number of GCM grid points that correspond to that region (von Storch et al. 1993; Corte-Real et al. 1995). The implications of this discrepancy have only been recognized recently and could undermine some results regarding regional climate change scenarios at a regional scale (Busuioc et al. 1999; Gonzalez-Rouco et al. 2000). One study in particular (Corte-Real et al. 1995) has shown that winter precipitation over Portugal is reproduced more successfully by applying one single

TABLE 3. Percentages of explained variance accounted for by the first six PCs of SLP for winter, spring, and autumn for periods 1901–90 observations only and 1941–90 observations and GS run.

	Winter			Spring			Autumn		
Mode	1901–90	1941–90	GS	1901–90	1941–90	GS	1901–90	1941–90	GS
PC1	33	35	38	28	30	35	21	21	29
PC2	19	18	20	15	15	17	17	17	18
PC3	16	16	14	14	13	12	16	16	16
PC4	12	12	12	13	13	11	12	12	12
PC5	4	5	5	6	7	6	7	7	6
PC6	4	4	4	6	5	5	6	5	5
Cumulative	88	90	93	82	83	86	79	78	86

TABLE 4. Correlations coefficients between the first six PCs for the observed 1901–90 SLP field and the projections (PRs) of the 1901–90 SLP onto the first six EOFs of the observed SLP for the period 1941–90. The highest value for each row is highlighted in bold.

	Winter						Spring						Autumn					
Mode	PR1	PR2	PR3	PR4	PR5	PR6	PR1	PR2	PR3	PR4	PR5	PR6	PR1	PR2	PR3	PR4	PR5	PR6
PC1	**0.99**	0.04	−0.01	0.00	0.01	0.03	**0.99**	−0.07	0.01	−0.06	−0.03	0.02	**0.91**	−0.40	−0.01	0.07	0.04	−0.01
PC2	0.03	**0.84**	0.53	0.04	0.01	−0.03	0.10	**0.99**	0.03	0.07	−0.02	0.03	−0.40	**−0.72**	0.57	−0.01	0.03	0.04
PC3	0.02	−0.61	**0.79**	0.10	0.02	0.02	0.08	0.10	**−0.97**	0.17	0.03	0.12	0.28	0.55	**0.79**	−0.02	0.04	0.02
PC4	−0.01	0.04	−0.17	**0.98**	0.05	0.00	0.04	−0.12	0.17	**0.97**	−0.04	0.07	−0.05	0.11	0.11	**0.98**	0.01	−0.01
PC5	−0.05	−0.03	−0.01	−0.11	**0.98**	0.09	0.00	0.03	0.08	−0.03	**0.96**	0.21	0.02	0.05	−0.05	−0.05	**0.99**	−0.06
PC6	−0.09	0.10	0.07	0.11	−0.17	**0.96**	−0.07	−0.10	0.24	−0.17	−0.33	**0.88**	−0.07	−0.05	−0.03	−0.02	0.19	**0.79**

downscaling model to estimate the area mean precipitation than by constructing many downscaling models (one for each station) and then averaging the results.

In fact, it is not entirely clear whether GCMs simulate point precipitation or area averaged precipitation (Skelly and Henderson-Sellers 1996; Osborn 1997; Osborn and Hulme 1998). The latter view, that is, that the GCM precipitation output has the statistical characteristics of an area-averaged precipitation time series, is probably more widely accepted by the scientific community (Osborn 1997; Busuoic et al. 1999). In the present study, we argue that if GCM precipitation output corresponds to an area averaged value, then it should ideally be compared with gridded present-day precipitation data. This has two important practical implications for regional climate change assessments:

1) Comparisons between direct GCM precipitation and observations should be made on a gridbox basis, that is, observed values should first be averaged for the same grid box as the GCM.
2) Comparisons between climate change scenarios based on direct GCM output and on downscaling techniques should also be made on a gridbox-scale basis, that is, even if a scenario is produced for each station, then it is more appropriate to average results within each grid box, prior to comparison.

In conclusion, all comparisons here will be carried out at the GCM gridbox scale. Thus, observed precipitation data will always be scaled up to the grid box, and more important, all downscaling models will be developed and validated for each grid box over Iberia (Fig. 1).

Recently, most of the work done in developing precipitation scenarios, either from direct output or downscaled, has been devoted to the daily scales because this corresponds to the needs of many potential end users (e.g., agricultural, water supplies, or energy production companies). However, monthly precipitation scenarios at the gridbox scale are still of the utmost relevance. Besides their interest per se, they are also used to feed many stochastic models, for example, weather generators (Semenov and Barrow 1997; Barrow et al. 1996) as well as an increasing number of different types of applied models in hydrology, natural vegetation, food production, etc., (Hulme et al. 1999; Arnell 1999; Harrison and Butterfield 1996).

The main objectives of this paper are twofold: first, to evaluate the performance of linear and nonlinear downscaling methods in developing scenarios of monthly precipitation at the gridbox scale; and second, to compare future regional trends in precipitation obtained with raw GCM data and downscaled results. Most previous authors have concentrated their attention only on the winter season (Table 1); here we extend the analysis to the other two main rainy seasons over Iberia: spring and autumn.

In section 2 we describe the datasets used in this work.

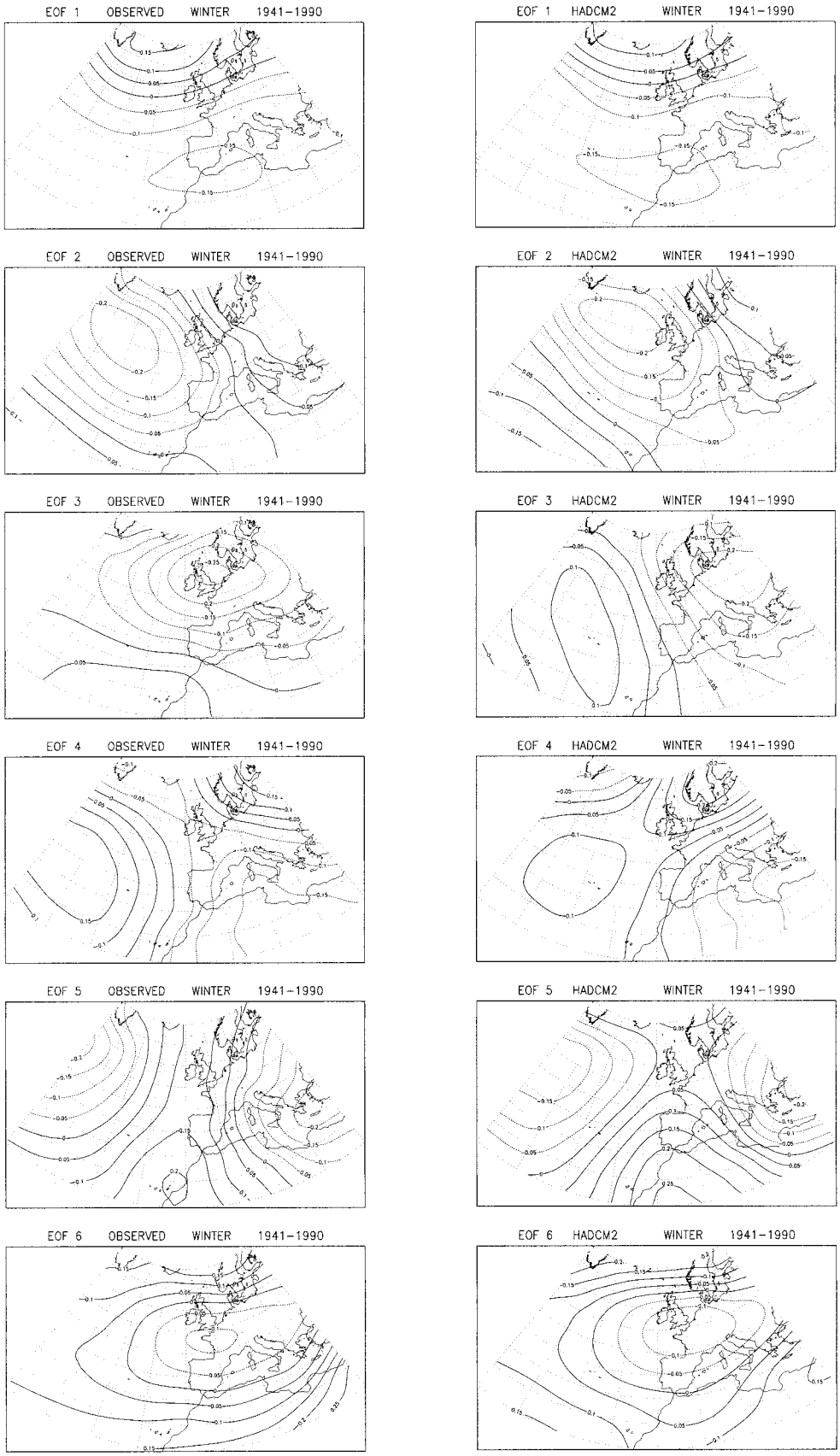
EOF 1 OBSERVED WINTER 1941–1990
EOF 1 HADCM2 WINTER 1941–1990
EOF 2 OBSERVED WINTER 1941–1990
EOF 2 HADCM2 WINTER 1941–1990
EOF 3 OBSERVED WINTER 1941–1990
EOF 3 HADCM2 WINTER 1941–1990
EOF 4 OBSERVED WINTER 1941–1990
EOF 4 HADCM2 WINTER 1941–1990
EOF 5 OBSERVED WINTER 1941–1990
EOF 5 HADCM2 WINTER 1941–1990
EOF 6 OBSERVED WINTER 1941–1990
EOF 6 HADCM2 WINTER 1941–1990

Then in section 3 we apply principal component analysis (PCA) to the observed and GCM-modeled SLP. An objective comparison of the mean observed and modeled SLP field is presented in section 4. The validation and comparison of linear and nonlinear ANNs downscaling models is described in section 5. Also in section 5, a stochastic model is fitted to the errors in the linear ANN model in order to improve the downscaled results. Section 6 describes the application of the best of the downscaling models to present-day and future GCM output and discusses the results of the developed scenarios. Some conclusions are presented in section 7.

2. Datasets

a. Observed and modeled sea level pressure

Observed (gridded): Observed monthly SLP was extracted from the Met Office dataset over an area from 25° to 65°N and from 50°W to 30°E (Jones et al. 1993). This dataset has a relatively coarse resolution (10° lat by 5° long). Such a low resolution is still appropriate for the computation of empirical orthogonal functions (EOFs) over a large area and represents a compromise in order to obtain a longer time series of SLP [the higher-resolution National Meteorological Center (now known as the National Centers for Environmental Prediction) gridded data only extend back to 1928]. The total period considered here was from 1901 to 1990.

Modeled (gridded): Monthly SLP data were extracted from two different runs of the Hadley Centre coupled ocean–atmosphere Unified Model (HadCM2; Johns et al. 1997). The greenhouse gases (GG) run is forced with historically increasing greenhouse gases for the 1861–1990 period and thereafter by a compound 1% yr^{-1} increase in effective carbon dioxide from 1991 to 2090 (similar to the IS92a scenario of Leggett et al. 1992). The GG-and-sulfates run (GS) has, in addition to the previous forcing, a representation of the direct radiative effect of sulfate aerosols (Osborn et al. 1999). Here, we concentrate on the GS run, because this experiment was designed to reproduce the actual climate system as faithfully as possible.

HadCM2 has a spatial resolution of 2.5° latitude by 3.75° longitude (Johns et al. 1997) and so the data had to be interpolated to the same resolution as the observed. Two distinct periods are used, a present-day period from 1941 to 1990 and a future period to assess future climate changes from 2041 to 2090.

b. Observed and model precipitation

Observed: Monthly precipitation is taken from the global land area precipitation dataset (Hulme 1992, 1994), available for the period 1901–90 and gridded at 2.5° latitude by 3.75° longitude, the same as the HadCM2 grid resolution. It is worth mentioning that this land area precipitation dataset includes, for the whole period, data from more than 40 stations located in the Iberian Peninsula, with an average of six stations per grid box (Rocha 1999).

Modeled: In order to be consistent with the corresponding periods of SLP data taken from the GCM, monthly precipitation from two distinct periods of both the GG and GS runs is used: a contemporary period from 1941 to 1990 and a future period from 2041 to 2090.

c. Comparison of observed and modeled precipitation

The area of study in this work is the whole of the Iberian Peninsula, that is, the continental territories of Portugal and Spain. This area corresponds to roughly nine grid boxes of the HadCM2 model and also of the Hulme precipitation dataset (Fig. 1). The grid boxes were numbered from Iberia 1 to Iberia 9.

It will be shown in this section that HadCM2 (GS run) has a low capacity to reproduce the observed regime of monthly precipitation for most of Iberia. Figure 1 shows the seasonal cycle of observed and modeled monthly precipitation averaged over the period 1941–90. In order to keep Fig. 1 comprehensible we restricted the explicit graphical representation to the four Iberian corners. From these it is possible to conclude the following:

1) The GCM is too wet in the northeast and northwest ''corners'' of Iberia, roughly corresponding to the Spanish provinces of Galicia and Catalonia, respectively.
2) The GCM is too dry over the two southern corners of the Iberian Peninsula. In other words, the model is exaggerating the observed north–south precipitation gradient (notice the different vertical scales on the graphics for the northern and southern regions).
3) The GCM minimum summer precipitation amount is always a month later (August) than the corresponding observed minimum month (July); that is, HadCM2 is unable to reproduce the correct timing of the driest period of the year.

Seasonal means and standard deviations for observations and HadCM2 output were computed for all nine grid boxes of Iberia. Results obtained for the three seasons with useful precipitation amounts (winter, spring, and autumn) can be observed in Table 2. Seasonal means and variances were tested using a two-tailed t test and F test, respectively. The significance level for rejection

←

FIG. 2. First six EOFs of winter SLP calculated from monthly data for the period 1941–90. Observations are shown in the left-hand column and HadCM2 GS in the right-hand column.

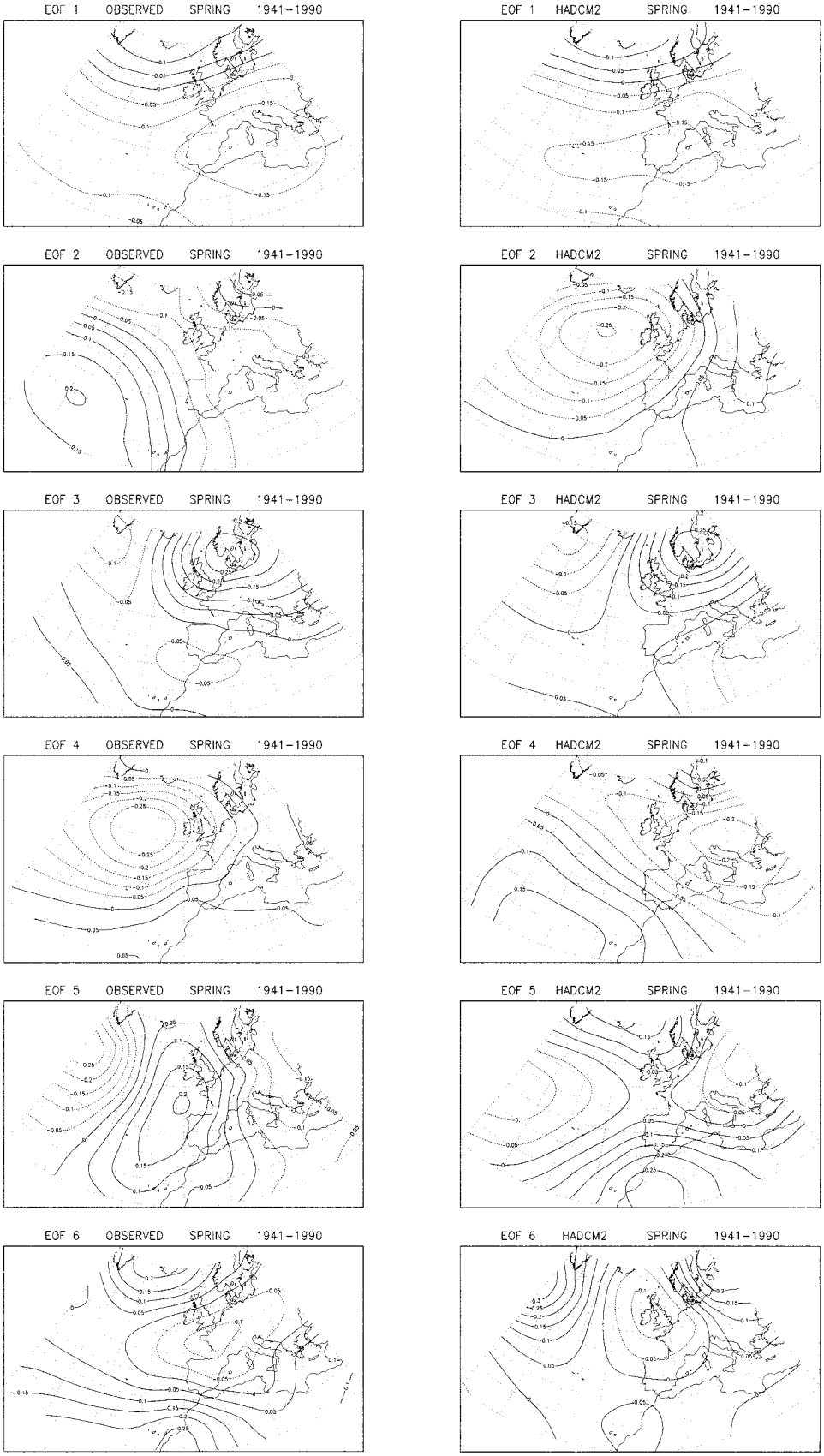
EOF 1 OBSERVED SPRING 1941–1990
EOF 1 HADCM2 SPRING 1941–1990
EOF 2 OBSERVED SPRING 1941–1990
EOF 2 HADCM2 SPRING 1941–1990
EOF 3 OBSERVED SPRING 1941–1990
EOF 3 HADCM2 SPRING 1941–1990
EOF 4 OBSERVED SPRING 1941–1990
EOF 4 HADCM2 SPRING 1941–1990
EOF 5 OBSERVED SPRING 1941–1990
EOF 5 HADCM2 SPRING 1941–1990
EOF 6 OBSERVED SPRING 1941–1990
EOF 6 HADCM2 SPRING 1941–1990

of the null hypothesis was set to 5% for both tests. Most grid boxes show significant differences between mean modeled and observed precipitation in all three seasons. Such discrepancies are also present for the standard deviation values, but with slightly fewer significant differences than are found for the mean in winter and spring.

The GG run presents a similar incapacity to reproduce the seasonal means and variances of precipitation throughout Iberia (results not shown).

3. Main modes of atmospheric circulation

a. PC analysis of observed SLP

The main modes of lower-troposphere circulation in winter over the Northern Hemisphere have been known for some time (e.g., Wallace and Gutzler 1981). Because of their relevance for Europe, the study of such circulation patterns over the North Atlantic and European sector has been particularly intensive both from diagnostic (e.g., Barnston and Livezey 1987) and modeling (e.g., Glowienka-Hense 1990; Corte-Real et al. 1995) perspectives. In recent years there has been a growth in studies constructing climate change scenarios over Iberia based on downscaling procedures (Table 1) using a range of different techniques (von Storch et al. 1993; Corte-Real et al. 1995; Cubasch et al. 1996; Corte-Real et al. 1999). Interestingly, most of these studies have one common step in their methodology: performance of a PCA of SLP. There are at least four important characteristics of this linear eigenvalue technique that justify its use in this context:

1) PCA is a relatively simple but effective tool to identify the main large-scale atmospheric circulation patterns (Barnston and Livezey 1987).
2) Usually, just a small number of PCs can capture most of the variance, thus greatly reducing the potentially large number of variables required to characterize the whole spatiotemporal variability of a dataset.
3) The main modes of spatial variability (EOFs) present a structure that is orthogonal, and so their associated PCs are uncorrelated with each other. This fact is extremely important if the researcher intends to use the time series of PCs as predictors in any type of transfer function–based downscaling model (Shubert and Henderson-Sellers 1997).
4) The present generation of Hadley Centre GCMs has revealed a good capacity to reproduce the winter spatial modes of variability (as depicted in a PCA) over the region under study (e.g., Osborn et al. 1999; Corte-Real et al. 1999).

The authors referred to above (Table 1) have confined their studies to the winter season (usually defined between December and February). Here this analysis will be extended to the other two relevant seasons (spring and autumn). Summer months are excluded not just because of their minor contribution to annual precipitation throughout Iberia (see Fig. 1) but also because of the convective nature of a large proportion of summer rainfall, that is, most of Iberian summer precipitation is not directly associated with the large-scale atmospheric circulation.

Although PCA has been extensively used in climatology, researchers do not agree on how to proceed at several intermediate steps of the analysis (Jolliffe 1990, 1993), namely, the following:

1) Should the covariance or the correlation matrix be used?
2) Should rotated or nonrotated components be used?
3) How many PCs should be retained?

The answers to each of these questions may depend on the specific type of analysis and the input data (Wilks 1995). In the present case the following options were selected:

1) The correlation matrix, to account for the different ranges of SLP variability observed at different latitudes.
2) Nonrotated components because, first, the first few EOFs retained (accounting for most of the variability) can be physically interpreted; and, second, the important property of noncorrelation between PCs, and the orthogonality of loadings, may be lost after rotation (Jolliffe 1993).
3) The third question is probably the most difficult one to answer. Different empirical rules have been applied to define the ''correct'' number of PCs to be retained. There is no single criterion that can be used to choose the number of PCs that ought to be retained in any given situation (Wilks 1995). It is a common procedure to retain all variables until the total explained variance reaches a certain threshold, typically on the order of 80% or 90%. Another possibility is to retain all PCs that individually account for more variation than the average variation in the original dataset, that is, to keep all PCs with corresponding *eigenvalues* higher than unity (Kaiser's rule). Such empirical rules are, by their very nature, subjective and can lead to different interpretations by different authors. In the present analysis an objective rule was applied, based on what is hopefully a more reliable statistical approach. The objective ''N rule'' divides the total variability into ''signal'' and ''noise'' components (North et al. 1982; Preisendorfer 1988). In this analysis only the signal

←

FIG. 3. As in Fig. 2 but for spring.

TABLE 5. Correlation coefficients between the first six PCs of the GS run (1941–90) and the projections (PRs) of the GS simulated SLP onto the first six EOFs of the observed seasonal SLP for the period 1941–90. The highest value for each row is highlighted in bold.

	Winter						Spring						Autumn					
Mode	PR1	PR2	PR3	PR4	PR5	PR6	PR1	PR2	PR3	PR4	PR5	PR6	PR1	PR2	PR3	PR4	PR5	PR6
PC1	**0.99**	−0.13	0.00	0.05	0.02	0.05	**0.99**	−0.13	−0.01	0.01	0.01	0.01	**0.90**	−0.40	0.05	0.14	0.06	−0.01
PC2	0.34	**0.92**	−0.07	−0.16	0.11	0.00	−0.01	−0.03	0.26	**0.91**	−0.27	0.06	−0.07	−0.05	**0.98**	−0.17	−0.03	0.04
PC3	−0.01	0.01	**0.96**	−0.25	0.02	0.07	0.01	−0.16	**−0.89**	0.40	0.09	−0.04	0.54	**0.82**	0.09	0.08	−0.07	0.03
PC4	−0.01	0.41	0.22	**0.85**	−0.22	0.04	0.19	**0.95**	0.14	0.05	0.15	−0.07	−0.32	0.07	0.20	**0.92**	0.01	−0.09
PC5	0.01	−0.24	0.21	0.55	**0.76**	−0.05	−0.18	−0.42	0.24	0.26	0.45	**−0.67**	0.21	0.30	0.11	−0.08	**0.74**	−0.51
PC6	−0.34	0.03	−0.17	0.01	0.02	**0.91**	−0.21	−0.25	0.08	0.11	**0.60**	0.45	−0.20	0.21	0.13	0.09	0.56	**0.51**

components are retained, that is, those PCs that are statistically significant at the 5% level.

PCAs were performed independently for the winter, spring, and autumn seasons for the entire 1901–90 period. A similar procedure was conducted for a shorter period; 1941–90, allowing for the study of the stability of the derived spatial modes (EOFs) and their associated explained variances. It will be shown that results obtained for the two periods are in fact very similar. The spatial window used corresponds to the whole area of data extracted from the observed dataset, that is, the area 25°–65°N by 50°W–30°E (see, e.g., Fig. 2).

The number of PCs obtained that are statistically significant at the 5% level varies between 7 (winter), 8 (spring), and 9 (autumn). However, the same analysis performed on the shorter period dataset (1941–90) identifies only 6 (winter) and 7 (spring and autumn) statistically significant PCs. It is important to keep in mind that the length of the time series used and the size of the window being analyzed are two important factors that affect the number of degrees of freedom (Richman 1986), thus altering the significance levels and hence the number of PCs to be retained. This means that the use of a longer (or shorter) time series or of a larger (or smaller) window will always imply a slightly different set of EOFs and their respective PCs. Taking this fact into account, and also the difficulty in interpreting the synoptic characteristics of the modes above No. 6, the number of modes retained for the present study, was restricted to the first six PCs for all three seasons. It is important to mention that the use of empirical rules, such as retaining all the modes with eigenvalues above one, implies many more PCs being retained, especially for spring and autumn.

The spatial patterns (EOFs) for these six modes of variability are shown for observed SLP in the left column of Figs. 2 (winter), 3 (spring), and 4 (autumn). The explained variances associated with the corresponding time series (PCs), for both the long and the short period, are shown in Table 3. The main features for each one of the first six modes can be summarized as follows (explained variance values are those of the 1901–90 analysis):

1) The first mode of variability (EOF1) in winter, spring, and autumn corresponds to the North Atlantic oscillation (NAO) pattern of circulation, and is associated with the presence or absence of strong zonal circulation (van Loon and Rogers 1978; Barnston and Livezey 1987). It explains 33% of the variance in winter, 28% in spring, and 21% in autumn.
2) The second mode of variability (EOF2) in winter (fourth in spring and autumn) is associated with the localization of high/low central pressure south of Iceland, extending to affect the west coast of Europe. It corresponds approximately to the east Atlantic (EA) pattern described in the literature (Barnston and

TABLE 6. Performance of downscaling approaches obtained with the linear and the 1 + 1 and 5 + 1 ANN models for winter, spring, and autumn, measured by correlation coefficients (multiplied by 100) between the observed and reconstructed precipitation time series for each grid box. Results for the nonlinear ANN models show the mean and the std dev (values in parentheses) of the correlations coefficients obtained with ensembles of 20 runs. The last two rows show the average results for all grid boxes and the first six, respectively.

	Winter			Spring			Autumn		
	Linear	1 + 1 (20 runs)	5 + 1 (20 runs)	Linear	1 + 1 (20 runs)	5 + 1 (20 runs)	Linear	1 + 1 (20 runs)	5 + 1 (20 runs)
Iberia 1	84	86 (≈0)	66 (17)	76	77 (≈0)	54 (11)	75	77 (≈0)	51 (26)
Iberia 2	86	88 (≈0)	69 (11)	64	67 (≈0)	50 (7)	64	64 (≈0)	45 (13)
Iberia 3	80	81 (≈0)	62 (10)	55	52 (≈0)	39 (13)	50	52 (≈0)	29 (14)
Iberia 4	75	76 (≈0)	62 (10)	60	61 (≈0)	32 (17)	56	48 (≈0)	32 (12)
Iberia 5	78	80 (≈0)	60 (6)	48	41 (≈0)	31 (6)	49	43 (≈0)	31 (12)
Iberia 6	73	75 (≈0)	50 (12)	51	48 (≈0)	37 (9)	42	26 (≈0)	24 (13)
Iberia 7	62	57 (≈0)	42 (8)	51	49 (≈0)	19 (23)	56	45 (≈0)	30 (15)
Iberia 8	45	32 (≈0)	24 (8)	47	48 (≈0)	20 (9)	43	21 (≈0)	23 (5)
Iberia 9	35	32 (≈0)	12 (10)	37	9 (≈0)	13 (12)	32	23 (≈0)	7 (11)
Total 1–9	69	67 (≈0)	50 (10)	54	50 (≈0)	33 (12)	52	44 (≈0)	30 (13)
Total 1–6	79	81 (≈0)	62 (11)	59	57 (≈0)	40 (11)	56	52 (≈0)	36 (15)

Livezey 1987). This mode explains 19% of the variance in winter, 13% in spring, and 12% in autumn.

3) The third mode of variability (EOF3) in winter and spring (second in autumn) corresponds to a dipole situation with one center near the Azores and the other over northern Europe. This configuration is similar to the typical blocking configuration over western Europe. It explains 16% of the variance in winter, 14% in spring, and 17% in autumn.
4) The fourth mode of variability (EOF4) in winter (second in spring and third in autumn) is characterized by SLP anomalies with the same signal west of the Azores and over Scandinavia separated by a region of opposite values extending in a northwesterly direction from the Mediterranean Basin to include Iceland. This pattern explains 12% of the variance in winter, 15% in spring, and 16% in autumn.
5) The last two modes (EOF5 and EOF6) represent less important modes of spatial variability, accounting for only low values of explained variance (between 4% and 7%) in all three seasons.

TABLE 7. Skill scores of the linear ANN model compared with the monthly climatology for winter, spring, and autumn. The last two rows show the average results for all grid boxes and the first six, respectively.

	SS_{Clim}		
	Winter	Spring	Autumn
Iberia 1	63	51	52
Iberia 2	74	40	41
Iberia 3	58	30	24
Iberia 4	56	35	30
Iberia 5	60	23	24
Iberia 6	52	11	13
Iberia 7	33	24	28
Iberia 8	19	22	17
Iberia 9	10	12	10
Total 1–9	47	27	26
Total 1–6	60	31	31

b. The stability of the EOF patterns

As mentioned previously, the PCA methodology was applied to a longer (1901–90) and a shorter (1941–90) observational period. The reason is simple: all downscaling models developed in section 5 have to use the longer period, so that they have a sufficiently long time series for calibration and validation. However, a comparison between the PCA results obtained with the observed and GCM fields should be performed with equal length datasets. This comparison is presented in section 3c using the 50-yr shorter period data. Prior to carrying out this analysis, it is necessary to establish that the EOFs derived from the short period of observations have the same characteristics as the EOFs from the longer observed record.

One method to evaluate the spatial similarity between the main modes of atmospheric circulation variability obtained for two independent datasets is to use spatial correlation coefficients (Wilks 1995; von Storch and Zwiers 1999). However, such an approach does not take into account possible different length of the datasets. Another straightforward technique is to use the projection of the second dataset onto the EOFs computed from the first dataset (Corte-Real et al. 1995; Zhang et al. 1997). In the present case, such a procedure requires the computation of the correlation coefficients between the first six PCs of the 1901–90 observations and the projections (PRs) of the observed 1901–90 SLP field onto the EOFs of the observed 1941–90 SLP.

Results of this procedure are shown in Table 4. A perfect match between corresponding EOFs would be characterized by a correlation matrix between the PCs and PRs, with $r = 1.0$ (or $r = -1.0$) in the principal diagonal. Two EOFs with very different spatial patterns would be characterized by a correlation coefficient close to zero. In the table, the highest value for each row (PC) is highlighted in bold. The highest correlation values are all located on the main diagonal, that is, the *n*th PR

TABLE 8. Means and std devs of seasonal precipitation for all nine grid boxes, computed from 50 yr of observations and downscaled data from GS (values in parentheses) for 1941–90. Significant differences at the 5% level are highlighted with *.

	Winter		Spring		Autumn	
	Mean	Std dev	Mean	Std dev	Mean	Std dev
Iberia 1	136 (134)	88 (76)*	88 (90)	51 (46)	95 (100)	64 (54)*
Iberia 2	102 (102)	69 (77)*	70 (71)	42 (43)	71 (77)	59 (52)*
Iberia 3	81 (79)	57 (51)*	50 (51)	35 (33)	54 (63)	52 (47)
Iberia 4	70 (68)	34 (32)	64 (65)	28 (26)	69 (72)	37 (35)
Iberia 5	43 (43)	32 (28)	45 (45)	26 (24)	41 (44)	29 (27)
Iberia 6	67 (66)	53 (47)	50 (51)	36 (36)	47 (53)	43 (39)
Iberia 7	48 (46)	26 (26)	57 (46)	30 (28)	54 (55)	31 (28)
Iberia 8	36 (36)	30 (26)	38 (36)	30 (26)	60 (64)	50 (41)*
Iberia 9	25 (26)	21 (19)	24 (26)	20 (18)	35 (37)	31 (28)

for the longer period is always better related with the *n*th PC from the shorter period than with any other PC. The correlation coefficient for all three main diagonals are all greater than 0.7 and many times exceed 0.95, thus showing that the EOF patterns obtained for the two periods are indeed very similar (the negative signal is of no consequence because of the orthogonal character of EOFs). Poorer results are seen for three PCs in autumn (PC2, PC3, and PC6), with correlation coefficients between 0.7 and 0.8.

We conclude that it is reasonable to assume that the EOFs derived for the short period (Figs. 2, 3, and 4) are representative of the main modes of variability for the longer period (EOFs not shown). Furthermore, these results are in agreement with a similar analysis performed over the same region but using two nonoverlapping subsets of years (Corte-Real et al. 1995).

c. PC analysis of modeled SLP

The objective comparison between observed and GCM-derived EOF patterns is performed with the same approach used in the previous section. Correlation coefficients were computed between the first six PCs of the HadCM2 runs, for the 1941–90 period, and the PRs of the corresponding modeled SLP onto the EOFs of the observed (1941–90) SLP field. The results are shown in Table 5. The explained variance associated with each PC was presented in Table 3 to make comparisons easier with corresponding observed PCs.

1) WINTER

Figure 2 shows that EOF1 is well reproduced by the GCM—the corresponding correlation coefficient is $r = 0.99$ (Table 5). Despite this good spatial agreement, as shown earlier (Table 3) the model overestimates the observed variance of EOF1 by 5%. This overestimation of the variance associated with EOF1 is in agreement with results obtained by previous authors (Corte-Real et al. 1995; Busuic et al. 1999).

It is possible to infer from the bold numbers in the principal diagonal of Table 5 that all the remaining five EOFs are well reproduced by the model and in the correct order. This is again an important result because precipitation over Iberia does not depend only on the first mode of SLP variability. As shown in Table 5 the worst performance is for EOF5 ($r = 0.76$), the pattern where the southern ridge intrusion of positive SLP values in the GCM reaches higher latitudes than in the observed EOF (Fig. 2).

Generally, the PCs of the last five modes of variability present good agreement between the observed and the modeled explained variance (Table 3). However, the cumulative explained variance obtained by the first six GCM PCs (93%) is slightly higher than the corresponding observed total (90%). This small overestimation by the first six GCM PCs can also be found for spring and autumn.

2) SPRING

As in winter, the similarity between the observed and modeled EOF1 pattern is quite remarkable, with $r = 0.99$. However, as shown in Table 3, there is a 5% difference in the explained variance associated with the PC1 between the observed (30%) and the HadCM2 experiment (35%).

Unlike winter, the results for spring do not show the same PC order between HadCM2 and the corresponding PRs (Table 5). It can be observed in Fig. 3 that there are two exchanges. First, the observed EOF2 (EOF4) is similar to the modeled EOF4 (EOF2) and second, the observed EOF5 (EOF6) is similar to the modeled EOF6 (EOF5). Such exchanges in the order of the observed and modeled main modes can be partially attributed to the similar values of explained variance shared by the second and third and by the fifth and sixth observed

→

FIG. 4. As in Fig. 2 but for autumn.

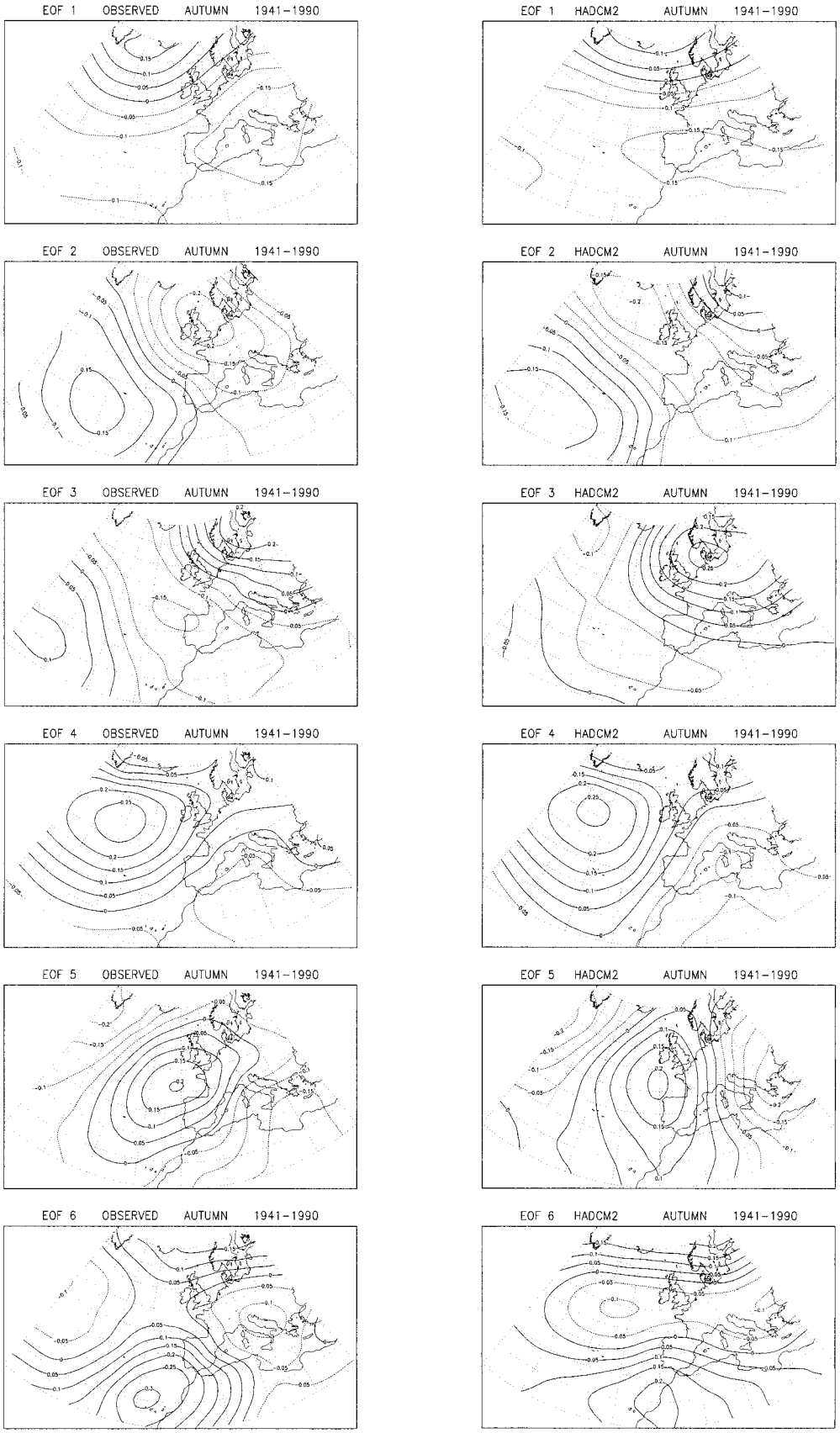
EOF 1 OBSERVED AUTUMN 1941–1990
EOF 1 HADCM2 AUTUMN 1941–1990
EOF 2 OBSERVED AUTUMN 1941–1990
EOF 2 HADCM2 AUTUMN 1941–1990
EOF 3 OBSERVED AUTUMN 1941–1990
EOF 3 HADCM2 AUTUMN 1941–1990
EOF 4 OBSERVED AUTUMN 1941–1990
EOF 4 HADCM2 AUTUMN 1941–1990
EOF 5 OBSERVED AUTUMN 1941–1990
EOF 5 HADCM2 AUTUMN 1941–1990
EOF 6 OBSERVED AUTUMN 1941–1990
EOF 6 HADCM2 AUTUMN 1941–1990

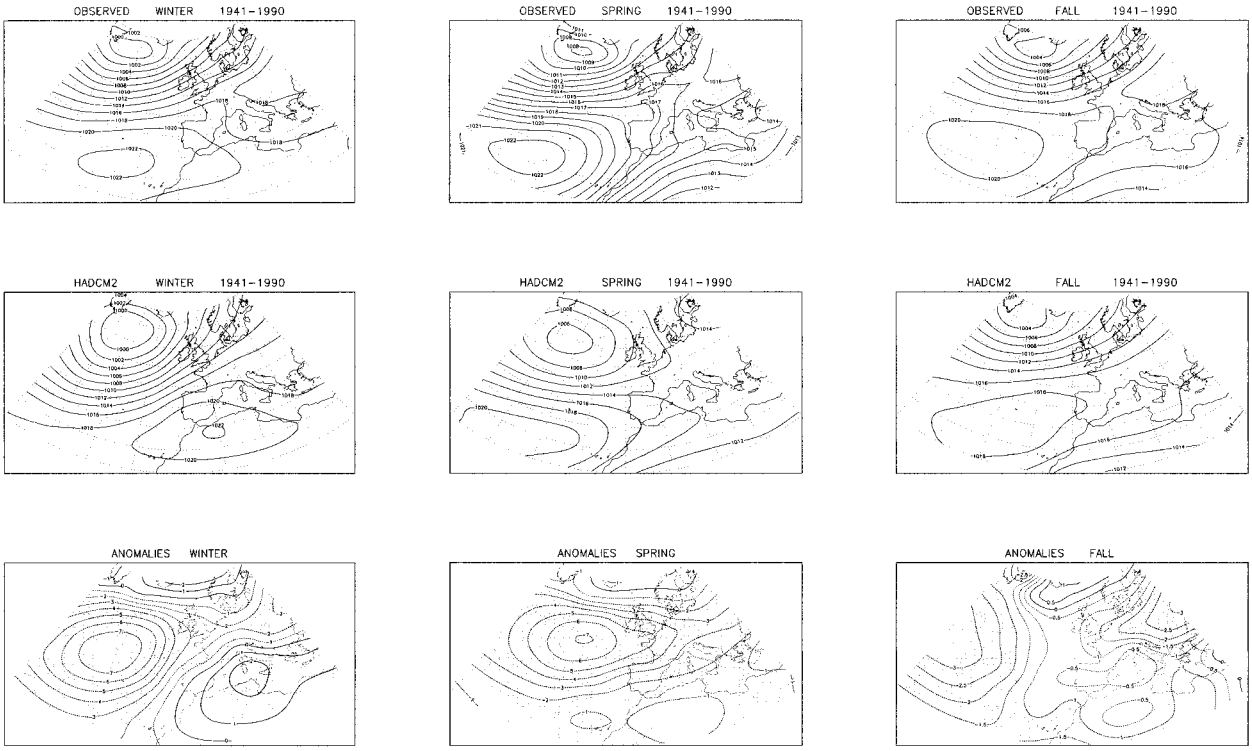

FIG. 5. The observed (first row) and modeled (second row) mean SLP field (GS) for winter (left), spring (center), and autumn (right). The third row shows the difference between the observed and modeled mean SLP fields. Zones where the difference field is different from zero at the 5% significance level are shaded.

modes (Table 3). As discussed earlier, a different sample (in length or size) can lead to a change of PC rank. However, it is worth mentioning that the respective correlation coefficients are high for all three cases ($r >$ 0.88), once the exchange between modeled EOF2 and modeled EOF4 is performed. The last two EOFs are not so well reproduced by the GCM, with correlation coefficients between 0.6 and 0.7, and both showing more than one statistically significant correlation.

3) AUTUMN

Unlike winter and spring, the similarity between the observed and modeled EOF1 patterns is good but not excellent in autumn, with $r = 0.90$ (Table 5). Furthermore, there is an even larger difference in the PC1 explained variance in this season (21% observed, 29% HadCM2) than in spring and winter (Table 3).

As in spring, results for autumn do not present the same order for PCs of modeled and observed PCs. There is one exchange: observed EOF2 (EOF3) is similar to modeled EOF3 (EOF2). This again can be explained in part as a sampling error due to very similar values of explained variance shared by these two modes (Table 3). The last two modes are poorly reproduced (especially EOF6), as shown in Fig. 4 and in Table 5, with PC6 being slightly better correlated with PR5 ($r = 0.56$) than with PR6 ($r = 0.51$).

4. The mean SLP field problem

The previous section has shown that HadCM2 is able to reproduce the main modes of atmospheric SLP variability with reasonable skill. It is worth noting that an objective comparison between GCM and observed predictor statistics is absent in many recent downscaling studies (e.g., Corte-Real et al. 1999; Gonzalez-Rouco et al. 2000). However, in order to apply properly any statistical downscaling methodology, the researcher must first be confident that the GCM can reproduce reasonably well not only the main modes of variability, but also the present-day average and variance of all predictor variables (Palutikof et al. 1997). Strangely, only one of the downscaling papers developed for the Iberia region and referred to in Table 1 presents a quantitative comparison of the observed and GCM SLP mean state (Goodess and Palutikof 1998). However, this study was performed with an earlier GCM version from the Met Office, the UKTR model run.

One possible simple way to evaluate the differences between observed and modeled data is to compute the difference of both mean states on a seasonal basis [e.g., Bürger (1996) for the ECHAM3 model; Goodess and Palutikof (1998) for the UKTR model]. Here, the comparison is completed by applying a two-tailed t test to the difference field.

The observed and GS mean fields, and the respective

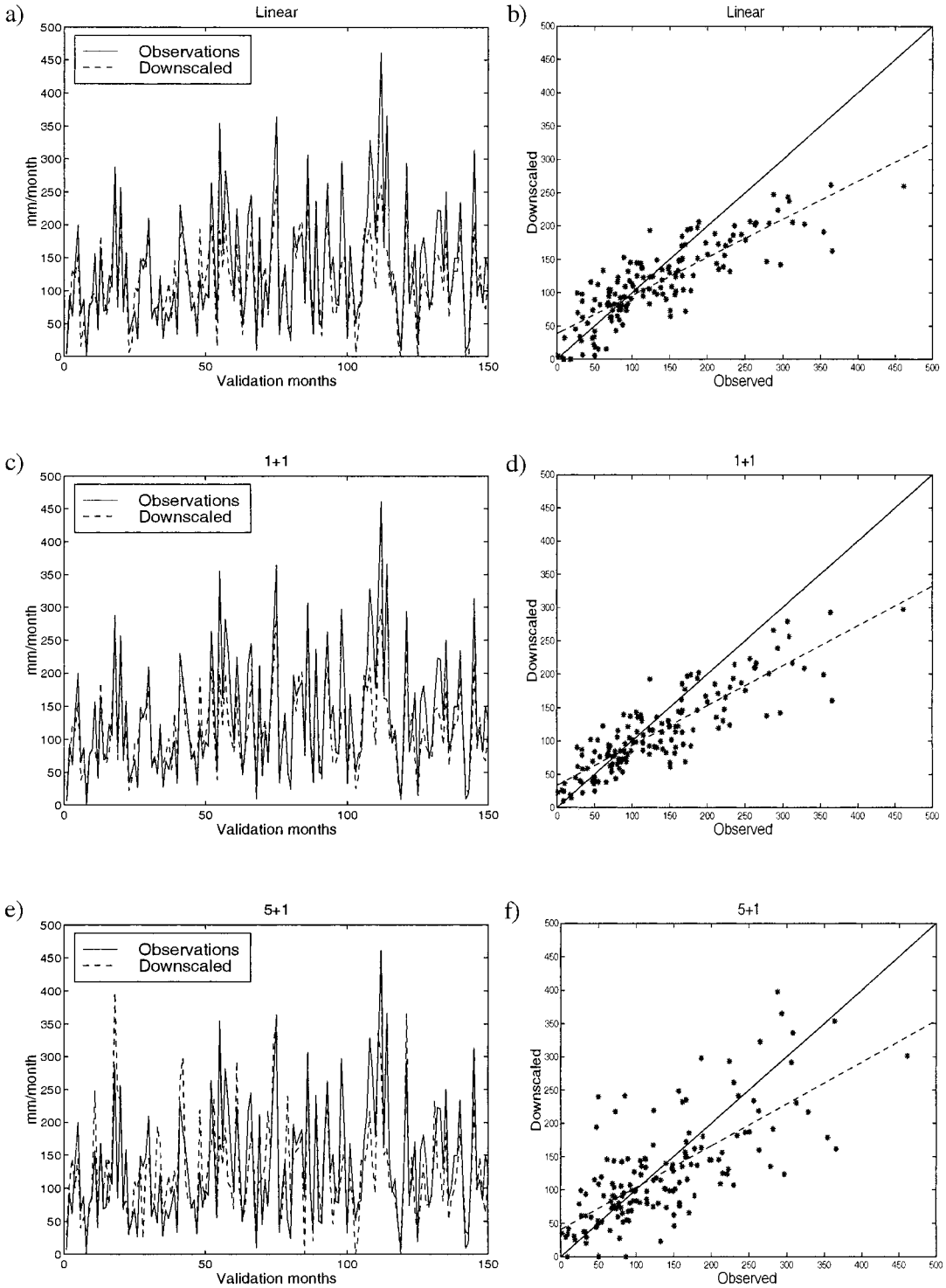

FIG. 6. Validation results for Iberia 1. The left-hand column shows monthly time series of observations and downscaled precipitation using the (a) linear, (c) 1 + 1, and (e) 5 + 1 models. The right-hand column shows the corresponding scatterplots for the (b) linear, (d) 1 + 1, and (f) 5 + 1 models.

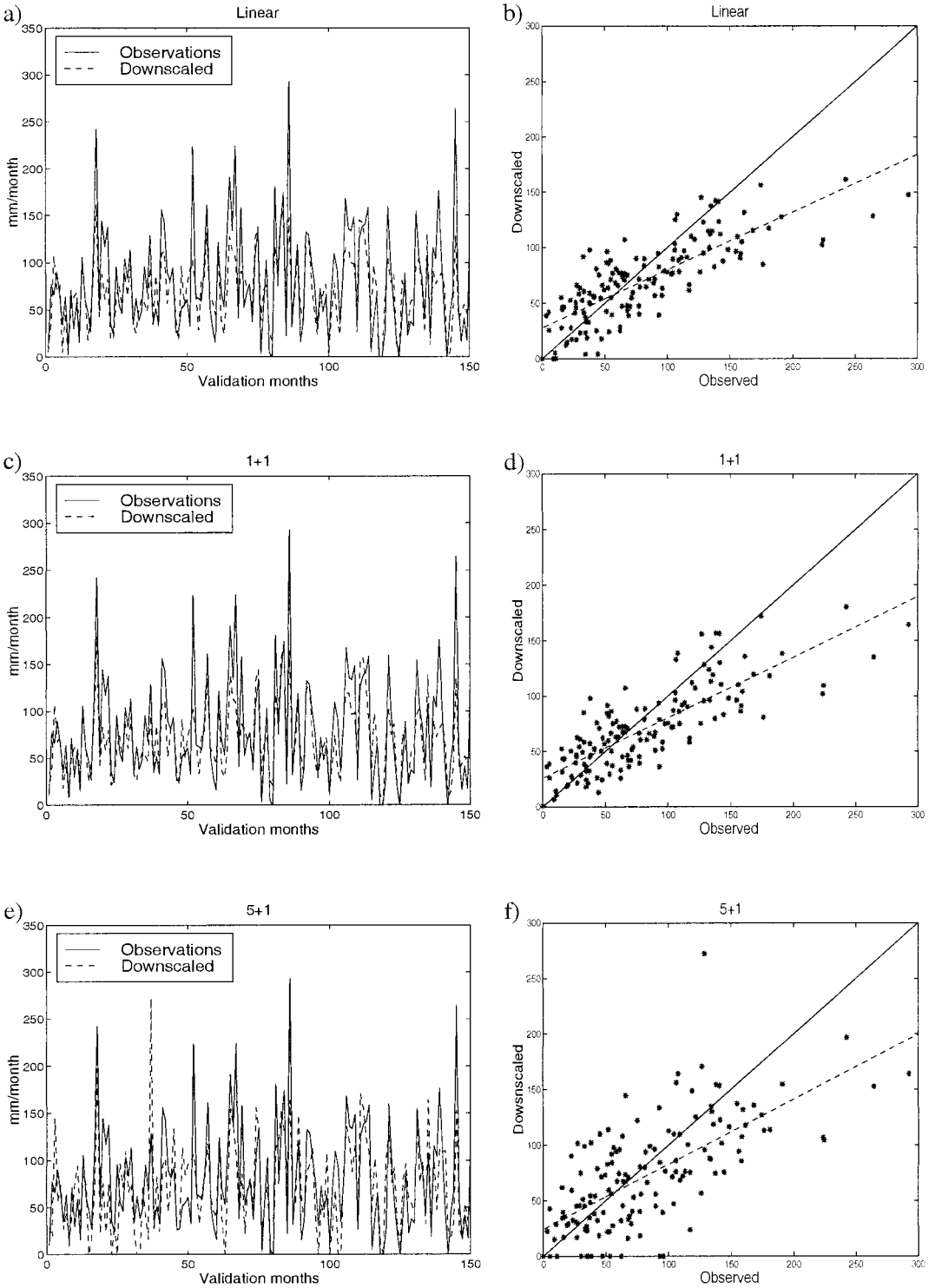

FIG. 7. As Fig. 6 but for Iberia 3.

difference fields, are shown in Fig. 5. Zones where the difference field is different from zero at the 5% significant level are shaded. In winter, the incapacity of the GCM to reproduce the Azores high is quite remarkable, while the Icelandic low extends unrealistically far to the south. This latter deficiency appears again in spring. Such deficiencies are responsible for a large region over the Atlantic Ocean where the SLP mean field is badly reproduced throughout the three seasons. The Iberian Peninsula area shows better results in winter and au-

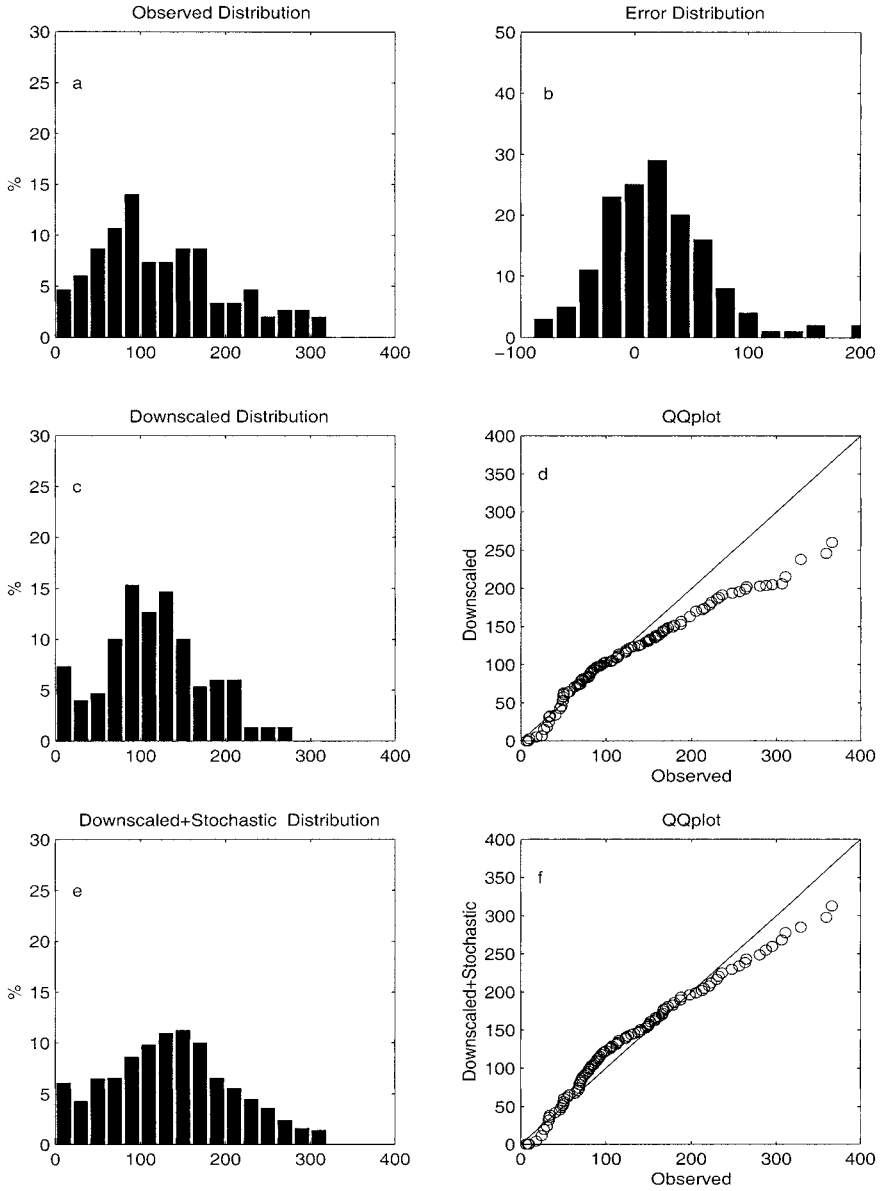

FIG. 8. (a) Observed monthly precipitation frequency distribution for Iberia 1, (b) distribution of the errors for the ANN linear downscaling model, (c) monthly precipitation distribution obtained with the downscaling procedure, (d) qq-plot of downscaled values vs observations, (e) monthly precipitation distribution obtained with the downscaled plus stochastic procedures, and (f) qq-plot of downscaled plus stochastic precipitation vs observations.

tumn, but still presents significant differences in spring. The magnitude of the winter difference field is similar to that obtained by Goodess and Palutikof for the UKTR model (only carried out for winter season).

This simple but essential analysis shows that, although the HadCM2 model is able to reproduce the main modes of SLP variability, it cannot successfully reproduce mean SLP for a large region over the Atlantic Ocean. This deficiency has been unnoticed in previous studies based on HadCM2 data (e.g., Corte-Real et al. 1999; Osborn et al. 1999). Probably the most important implication for scenario construction of the bias detected in the GCM mean state is the necessity to consider the present-day model climatology as a baseline rather than the present-day observed climatology. Such an approach has been widely used in the past to overcome the inability of GCMs to reproduce the mean SLP field (e.g., von Storch et al. 1993; Corte-Real et al. 1995).

Results obtained for GG are almost identical to those just described for GS. The GG run presents a similar capacity to reproduce the main modes of SLP and a similar incapacity to simulate the mean SLP field.

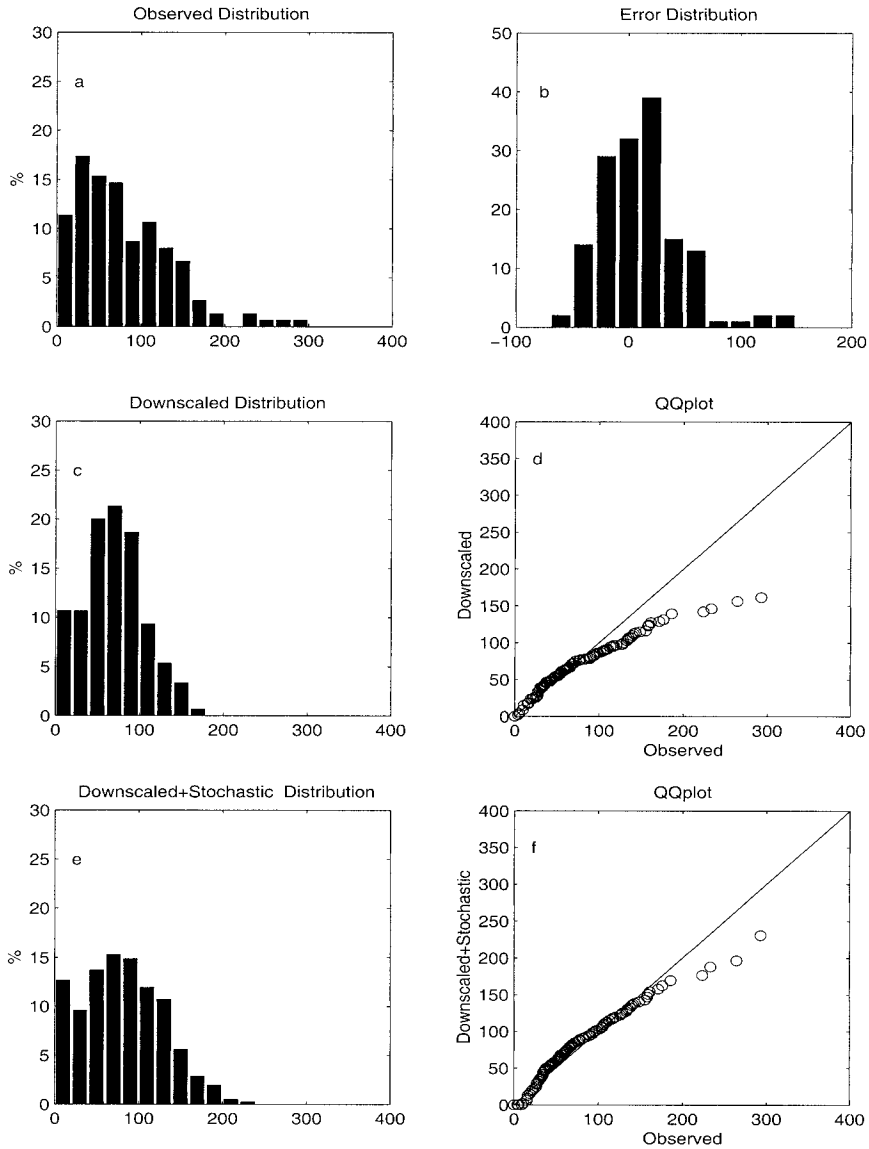

FIG. 9. As Fig. 8 but for Iberia 3.

5. The statistical models

Here, several linear and nonlinear ANN downscaling models are constructed using only observed SLP and observed precipitation data. It is intended that such models will be able to predict regional precipitation in each grid box using the PCs of SLP as predictors. The nonlinear ANN model adopted is the feed-forward configuration of the multilayer perceptron, and the training scheme is based on the optimized Levenberg–Marquardt algorithm (Hagan et al. 1996). The structure of the ANN models is similar to that used in TP99, that is, all nonlinear models have only two layers: one input layer with several nodes and one output layer with just one node. Hereinafter, this is referred to as having a $k + 1$ structure (i.e., $3 + 1$ structure implies the use of 3 nodes in the first layer and 1 node in the output layer).

The ANN results are analyzed in the next two sections. In order to keep to a minimum the number of figures and tables, the analysis focuses on the two westerly corner grid boxes, Iberia 1 and Iberia 3. These grid boxes were chosen because they represent typical wet (Iberia 1) and dry (Iberia 3) regions over Iberia. Furthermore, the precipitation seasonal cycle for both grid boxes was poorly reproduced by HadCM2 (Fig. 1), emphasizing the need for downscaling.

a. Validation of models

Both types of linear and nonlinear ANN models have been developed independently for each season, with the calibration and validation periods being 1901–40 and 1941–90, respectively [similar periods were recently

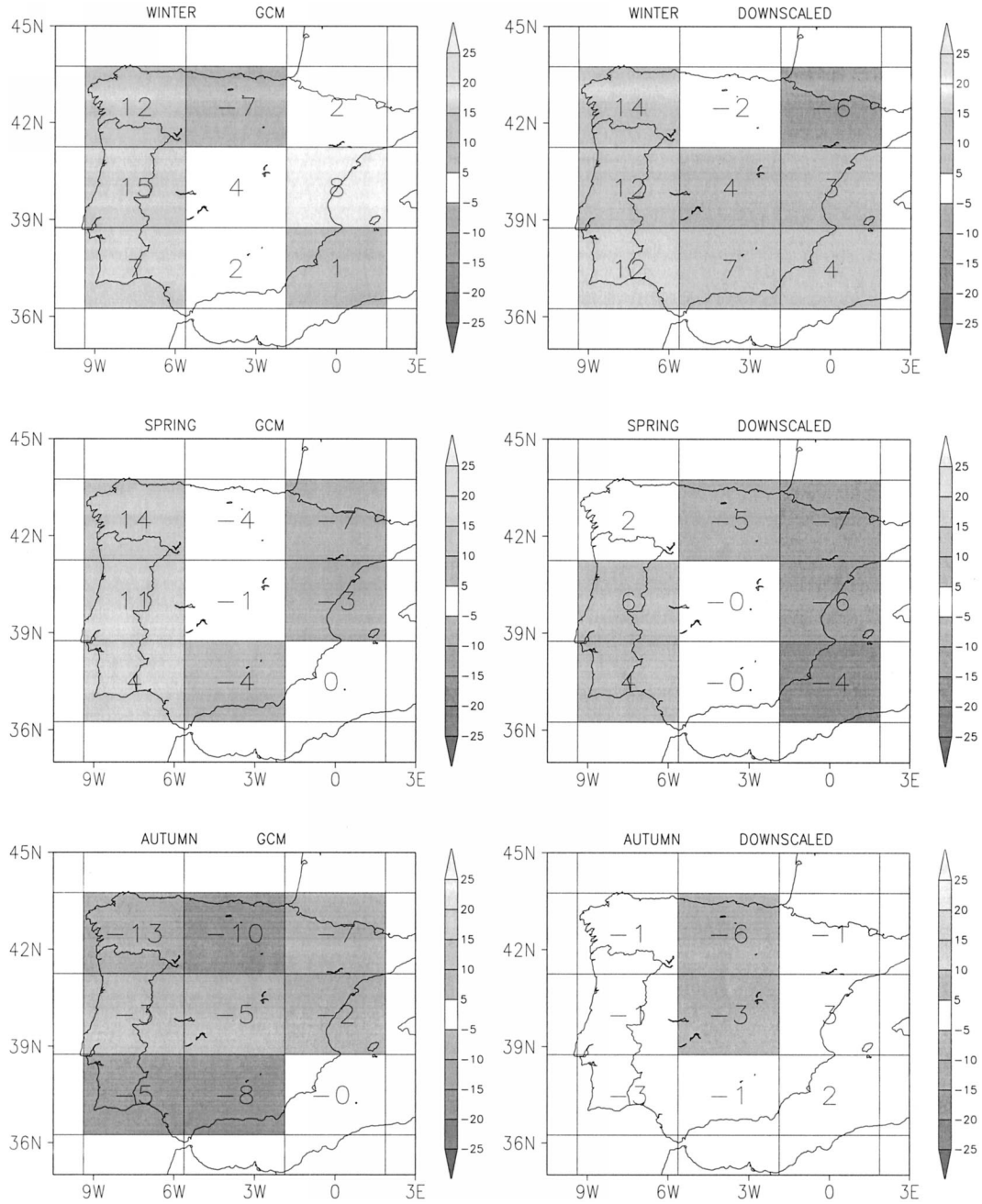

FIG. 10. Changes in seasonal gridbox precipitation between 1941–90 and 2041–90 obtained directly from the GS run (left-hand column) and from the downscaling procedure applied to GS (right-hand column, based on the linear ANN). Changes are shown in percentage (grayscale) and absolute values (mm month^{-1}) within each grid box.

used for a downscaling procedure over Romania by Busuioc et al. (1999)]. Here, the calibration and validations procedures will receive less emphasis than in TP99 (where additional validation techniques, including cross validation and bootstrapping, were used). Only the simple validation procedure from TP99 will be employed. Nonlinear ANN models are calibrated and validated with 20 different starting conditions, producing 20 potentially different results.

All the ANN models (linear and nonlinear) use PCs from observed SLP as input predictors. These PCs correspond to time series of the EOFs presented in the left-hand columns of Figs. 2, 3, and 4. Validation results for all Iberian grid boxes are shown in Table 6 and the corresponding validation plots for the Iberia 1 and Iberia 3 grid boxes (winter) can be seen in Figs. 6 and 7. The discussion here is based on correlation coefficients between the observed and the modeled

precipitation time series for each season of the validation period (1941–90). The dispersion of the nonlinear model results is given by the standard deviations of the correlation coefficients for the 20 ensemble members. The main conclusions to be drawn from Table 6 are as follows:

1) Results for western and central Iberia have higher correlations than those for eastern Iberia. The last two rows of each season show that the average correlation for the nine grid boxes is always smaller than the equivalent average for the first six grid boxes (western and central Iberia). The magnitudes of the results are in agreement with previous calibration-validation results for the region obtained using different downscaling approaches (von Storch et al. 1993; Gonzalez-Rouco et al. 2000).
2) Results from the linear or slightly nonlinear ANN models (1 + 1) show the highest correlation coefficients. This evaluation measure decreases steadily from the 1 + 1 to the 5 + 1 model, that is, results from the 2 + 1 model are worst than those obtained with the 1 + 1 model; results from the 3 + 1 model are worst than those from the 2 + 1 model; and so on (not shown). Furthermore, while the dispersion of results is virtually zero for the simplest 1 + 1 nonlinear model, it becomes quite large for the 5 + 1 model.
3) Interestingly, only when correlation values are relatively high does the 1 + 1 nonlinear model present slightly higher values than the linear model. For the eastern Iberian grid boxes, the 1 + 1 model is always weaker than the linear model.
4) As expected, spring and autumn models have lower correlation coefficients than the equivalent winter models. However, there is still a clear performance decrease from the linear and 1 + 1 version to the 5 + 1 model, accompanied by an increasing dispersion of correlation coefficients. As in winter, the spring and autumn models for eastern grid boxes have lower correlation values than the central and western grid boxes.

Two further examples of comparison between observed and downscaled winter precipitation are shown in Fig. 6 (Iberia 1) and Fig. 7 (Iberia 3). The left-hand columns show the monthly time series of the observed and downscaled precipitation values for the validation period (150 cases); the right-hand columns show the corresponding scatterplots. These reveal a typical problem of most statistical downscaling precipitation models; namely, a general inability to reproduce observed precipitation variability. This is demonstrated by the time series in the left-hand column, where a general failure to reach the high precipitation extremes is notable in the downscaled values.

The figures show that the 5 + 1 nonlinear model is somewhat better than the simpler models in reproducing higher-precipitation amounts. This ability of the 5 + 1 model is also responsible for a smaller bias—the regression line is closer to the 1:1 line than it is in the linear or the 1 + 1 models (right-hand column of Figs. 6 and 7). Despite this, the 5 + 1 ANN model is generally less accurate than the simpler models (as shown by Table 6). The spread of values around the regression line is similar for the linear and the 1 + 1 model and is higher for the 5 + 1 version. Although not presented, the general comments on Iberia 1 and Iberia 3 results apply to other grid boxes.

In conclusion, it seems evident that, in this case, the best ANN models are the simplest ones, that is, either the linear, or slightly nonlinear (the simple 1 + 1) version. It is worth mentioning that the linear ANN model corresponds to a multiple linear regression model and that an ANN model with only one nonlinear node is similar to the logistic regression equation (Sarle 1994). Based on these results, it was decided to adopt the simplest, linear, model. The linear ANN model results are not only reasonable but of similar quality to results from other downscaling techniques previously developed for Iberian monthly precipitation (Corte-Real et al. 1995; Zorita and von Storch 1999; Gonzales-Rouco et al. 2000).

The skill score associated with the ANN linear model is computed here during the validation procedure. The skill score is based on the mean square error (MSE) and uses the monthly climatological mean as the reference (Wilks 1995):

$$\mathrm{SS}_{\mathrm{Clim}} = \frac{\mathrm{MSE} - \mathrm{MSE}_{\mathrm{Clim}}}{0 - \mathrm{MSE}_{\mathrm{Clim}}} \times 100\%. \qquad (1)$$

Unlike daily temperature (TP99), the monthly grid box precipitation has weak autocorrelation values, implying that persistence is usually a poorer model than climatology. Thus, it is more important to evaluate the performance of the statistical downscaling models against climatology than against persistence. Table 7 summarizes the $\mathrm{SS}_{\mathrm{clim}}$ results obtained for every grid box for winter, spring, and autumn. Again, it is evident that the highest values of skill are attained for the western and central Iberian grid boxes. In general, winter results are better than spring and autumn. The spring and autumn seasons present similar values of skill throughout Iberia, and all seasons reveal the poorest results for the Iberia 8 and Iberia 9 grid boxes, in accordance with the poor correlation coefficient values for these two grid boxes in Table 6.

b. Adding a stochastic component

Several authors have recently shown that most downscaling models for precipitation tend to damp the observed variability, that is, they are unable to properly simulate extreme situations at daily (Bürger 1996; Hewitson and Crane 1998) or monthly (Zorita and von Storch 1999) scales. As seen in the previous section, this seems to be the case with both the linear and nonlinear ANN

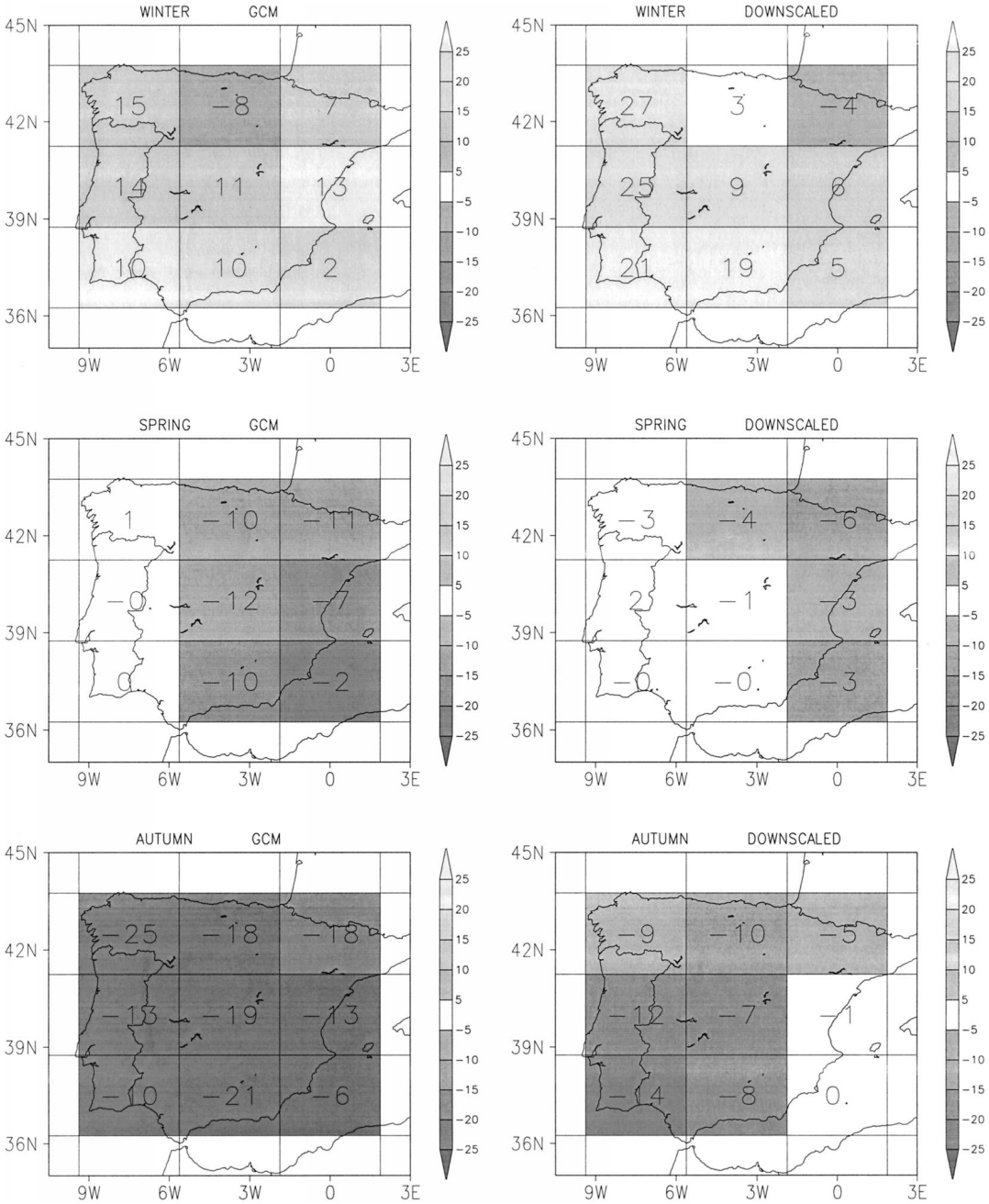

FIG. 11. As Fig. 10 but for the GG run.

models for monthly precipitation downscaling over Iberia. It was shown in section 5a that nonlinear ANN models can simulate higher values of variability and present smaller bias. However, this apparent increase of performance is obtained at the expense of lower values of explained variance (Table 6) and, consequently, higher values of root-mean-square error (not shown). These findings for the nonlinear models are in good agreement with those of previous authors (Bürger 1996; Zorita and von Storch 1999). Figures 8 (Iberia 1) and 9 (Iberia 3) show the frequency distributions for observed (Figs. 8a, 9a) and downscaled (Figs. 8c, 9c) precipitation. These two plots correspond exactly to the same linear model results presented in Figs. 6 and 7. The discrepancy is evident and even more striking in the qq-plot (Figs. 8d, 9d). For both grid boxes the downscaled model is unable to reproduce the observed distribution for precipitation values above 100 mm. These qq-plots compare percentiles of the empirical cumulative distribution function of the observations and model data (Wilks 1995).

Some authors have developed specific downscaling techniques to increase the downscaled variance such as the ''inflated'' (Karl et al. 1990) or ''expanded'' (Bürger 1996) downscaling approaches. However, recent literature has undermined the validity of such techniques (von Storch 1999). To overcome the poor reproduction of observed variability, Hewitson and Crane (1998) suggest the implementation of a stochastic postprocessing phase. This can be achieved through the fitting of an appropriate distribution to the residuals of the model at the validation stage.

The error distribution associated with winter Iberia 1 and Iberia 3 downscaling models can be seen in Figs. 8b and 9b. Both distributions reveal a slightly non-Gaussian shape, with a small tail to the right. Thus, a (two parameter) gamma distribution was fitted to each error distribution for each gridbox model. We computed the shape parameter (α) and the scale parameter (β) using an approximation to the maximum likelihood estimators based on the following simple statistic (Wilks 1995):

$$D = \ln(\overline{x}) - \frac{1}{n}\sum_{i=1}^{n} \ln(x_i), \tag{2}$$

where $\overline{x}$ is the sample estimate of the mean. Then, the two required parameters can be easily estimated:

$$\hat{\alpha} = \frac{1 + \sqrt{1 + 4D/3}}{4D}, \qquad \hat{\beta} = \frac{\overline{x}}{\hat{\alpha}}. \tag{3}$$

The existence of negative error values requires the addition of a large constant value (typically 1000) to make possible the fitting of the Gamma distribution. The two parameters were computed for every grid box for the error frequency distribution for the period 1941–90. Then, a Monte Carlo technique was applied to sample from the error distribution. These simulated values were generated 100 times for each grid box, with 150 ''time steps'' each (150 = 50 yr × 3 months). The 100 values at each step were then averaged and added sequentially to the downscaled values obtained with the analytical transfer functions. After simulating these values, the large constant value (used only to obtain the distribution parameters) was subtracted. The final precipitation distribution for the validation period for Iberia 1 and Iberia 3 can be observed in Figs. 8e and 9e, respectively. These indicate that for both grid boxes the downscaled plus stochastic precipitation distribution is closer to the observed distribution than is the downscaled only distribution. This is also shown by the corresponding qq-plots shown in Figs. 8f and 9f, where the downscaled plus stochastic distributions are closer to the ideal 1:1 line than the downscaled distributions (Figs. 8d and 9d).

In conclusion, it was found that the application of this second step to the linear ANN models improved the capacity of the downscaling models to reproduce the observed distribution. The main effect of this stochastic step is to allow a better reproduction of the statistical characteristics of the observed precipitation. In particular, the variance of gridbox precipitation is much more realistic than it would be if obtained by the transfer function alone.

However, there are two important points to note with respect to using a stochastic component as a postprocessing tool:

1) It is desirable that the deterministic downscaling component is able to explain the highest amount of precipitation variability, that is, the remaining unaccountable explained variance should be as small as possible. If this condition is fulfilled, the researcher is more confident that the unaccounted variance corresponds mainly to local factors that are impossible to relate to the large-scale flow or other atmospheric variables (e.g., topographic effects, land cover). In our view, it is more reasonable to expect that the contribution of such local factors will remain unchanged in a future warmer climate, than to expect stationarity of the relationship between the large-scale and local climate. This is the justification for using the same error distribution to introduce the stochastic component in both the present-day and future scenarios.
2) It should be stressed that these stochastic models do not introduce more information from a climate change scenario point of view. This is because the same error distribution that is constructed with observed data is then applied to present day and future scenarios. Thus, when computing the climate change signal between these two temporal windows, the stochastic component is the same in both, and has no effect.

6. Future changes in precipitation over Iberia

In this section an estimation of the changes in seasonal precipitation over Iberia is presented. Changes derived directly from the gridbox precipitation simulated by HadCM2 are compared with the changes obtained indirectly through downscaling. The downscaled models discussed in the following sections are constructed using a combination of the linear ANN transfer functions obtained in section 5a and the stochastic component developed in section 5b (although, as noted above, the latter step will not affect the size of the perturbation).

a. Present-day downscaling

The downscaling methodology applied to HadCM2 data is first evaluated by comparing present-day downscaled scenarios based on GCM output (1941–90) with observations. The comparison procedure is similar to that in section 2c, that is, a comparison of the mean and standard deviation for all grid boxes is presented.

Values of observed and downscaled seasonal mean

precipitation can be observed in Table 8. This table shows an improvement from the equivalent GCM direct output results (Table 2). In fact, the aggregate number of grid boxes in which the downscaled results are significantly different from observations decreases from 21 (in Table 2) to 0 (in Table 8). As shown in the previous section, this decrease is a consequence of the joint application of the linear downscaling ANN model component followed by the stochastic model. Equivalent values of observed and downscaled seasonal standard deviations are also shown in Table 8. In this case there is a more modest improvement from the direct GCM output results. The number of grid boxes with significant differences decreases from 17 to 6. The six significant occurrences tend to occur mainly in the western part of Iberia, especially during winter and autumn.

b. Construction of future precipitation scenarios

As shown in section 4, the present-day seasonal SLP climatology simulated by HadCM2 is in some respects dissimilar to the observed. In evaluating the future scenarios of precipitation we therefore use the present-day model climatology (1941–90) as a baseline rather than the present day observed climatology.

Seasonal changes obtained directly from the gridbox precipitation of the HadCM2 GS run are presented in the left-hand column of Fig. 10 while the equivalent changes obtained with the downscaling procedure are shown in the right-hand column. It was demonstrated earlier (Fig. 1) that the observed means and standard deviations of monthly precipitation over Iberia show large differences between regions. Thus, changes in precipitation are presented as both percentages (grayscale) and absolute values (number within each grid box). The most important results from Fig. 10 can be summarized as follows:

1) Generally, there is good regional agreement between the signs of the precipitation changes (either wetter or drier) in the GCM and the downscaled results, in all three seasons.
2) In winter most of Iberia experiences an increase using both approaches. This increase is more intense over the western grid boxes.
3) The grid box over mountainous north-central Iberia presents a small decrease in all three seasons.
4) Spring results show a consistent increase in the western part of Iberia, with smaller changes obtained for the downscaled approach. A decrease in eastern Iberia is predicted by both approaches, although the change is greater for the downscaling technique.
5) Results for autumn derived directly from the GCM shows a strong decrease for most grid boxes, whereas the downscaling approach presents a much smaller decrease throughout most regions of Iberia.

Because of the very different nature of both the underlying model experiments and the downscaling techniques employed by other authors, it is very difficult to place the present results within the broader context of earlier papers. Corte-Real et al. (1995) using the UKTR model obtained a decrease in winter precipitation over Portugal (western Iberia region), both with direct GCM output and by downscaling. This result is substantively different from those presented here for the western grid boxes of Iberia.

There appears to be some consistency between the present set of results and those of other authors using HadCM2, although with different downscaling techniques. A winter increase in western Iberia, particularly over Portugal, was documented by Palutikof et al. (1999). These authors have also shown a small increase of precipitation for the spring season over Portugal and a decrease in the eastern parts of Iberia. They find a generalized decrease in Iberian autumn precipitation, similar to the one shown in Fig. 10. These authors have used a totally different downscaling methodology, based on the use of terrain variables (latitude, longitude, altitude, distance to sea, etc.) with no information related to large-scale atmospheric dynamics. Another recent work based on HadCM2 (Gonzalez-Rouco et al. 2000) has provided similar results to those obtained in this section for winter. Not only do Gonzalez-Rouco et al. show a general increase of precipitation throughout most of Iberia, they also obtain a small decrease in the northern mountainous regions, near the Pyrenees.

Last, climate change scenarios based on the GG HadCM2 experiment were constructed. Seasonal changes in precipitation obtained directly from GG gridbox output are shown in Fig. 11 (left-hand column). The equivalent changes obtained with the downscaling procedure are shown in the right hand-column in Fig. 11. Important features are the following:

1) In general, the amplitude of the changes is higher than with GS. This is true for both direct GCM and downscaled results.
2) The winter increase is especially large for the downscaled scenario, with precipitation increases above 20% for most of the western and central grid boxes.
3) The spring scenarios, unlike those for the GS experiment (Fig. 10), do not show an increase over western Iberia.
4) The decrease of precipitation in autumn is spread throughout Iberia, and is stronger than in the GS experiment, with the direct GCM results suggesting a decrease greater than 25% in most grid boxes.

In summary, climate change scenarios derived from GG are of a similar nature to GS, but with larger differences from the present day climate. This result is perhaps to be expected given the nature of the two experiments. The seasonal cycle of precipitation in GG has an even greater concentration into a shorter winter season, with a larger range of interseasonal variability, as shown by the drier autumn and spring, in both the downscaled and direct scenarios.

7. Conclusions

The main conclusions from this paper can be summarized as follows:

1) HadCM2 is unable to simulate accurately present-day monthly precipitation over most of the Iberian Peninsula. Generally, this GCM has a tendency to be too wet in the northern regions of Iberia and too dry in the southern grid boxes. In particular, the simulated variability is much lower than observed.
2) A PCA performed on the observed SLP field on a seasonal basis allowed the identification of the most important circulation patterns (EOFs) and their respective time series (PCs). These were later used as predictors of Iberian precipitation in the downscaling models. The first EOF of the SLP field represents the NAO, one of the most significant large-scale patterns that controls European climate and, in particular, Iberian precipitation.
3) HadCM2 accurately reproduces the modes of atmospheric circulation obtained with the PCA. However, this GCM is incapable of reproducing the mean state of the SLP field.
4) Validation results for the linear and nonlinear ANN models reveal that the best ANN models are the simplest, that is, either the linear, or slightly nonlinear 1 + 1 version. However, the variability of downscaled precipitation is usually lower than observed, whichever ANN model is selected.
5) A stochastic model was constructed by fitting a gamma distribution to the model residuals in the previous step. The application of this stochastic step provides a better simulation of the present-day precipitation distribution throughout Iberia.
6) Generally, future climate change scenarios for Iberia indicate an increase of precipitation in winter and a decrease in autumn. This concentration of precipitation into a shorter ''wet'' season is specially prominent with GG.
7) Overall, there is reasonable agreement between the scenarios obtained from direct GCM output and by downscaling. However, the magnitude of change tends to be higher in the former than in the latter.

From a technical point of view, the most important conclusion is that results cannot be improved using more complex ANN models. There might be a relatively simple factor preventing an improved performance from more complex nonlinear ANN models. For example, it is possible that the successful application of more complex ANN models to downscaling problems depends critically on the quality of the association between the available predictors and the predictand. Unlike the consistently high values of explained variances obtained in validation of daily Tmax and Tmin, downscaling models presented in TP99 (where most explained variance values were above 80%), the explained variance for the present precipitation models is modest (<65%). Thus, it might be argued that there is, for each different downscaling problem, a minimum threshold of explained variance in order to successfully apply a more complex nonlinear ANN model.

It has been shown recently that the use of additional predictor variables can make an impact when downscaling with ANN models (Hewitson and Crane 1996: Crane and Hewitson 1998). Thus, a possible way to improve the performance of the statistical downscaling schemes developed in this work (making the use of nonlinear ANN models more attractive), would be to incorporate further large-scale information. Such information could be obtained from circulation indices defined at additional pressure levels, or from indices related to the atmospheric moisture content, the radiation balance and cloudiness. Unfortunately, such information is generally not available in either observed or GCM archives for sufficiently long periods to permit proper calibration and validation of the models. Thus, it is no surprise that the vast majority of work published in the last decade has seen the use of potential predictors restricted to the SLP and/or 500-hPa geopotential height indices. The recent development of the National Centers for Environmental Prediction and European Centre for Medium-Range Weather Forecasts reanalyses datasets and the storage of more GCM variables will improve, in the near future, the representation of physical processes related to precipitation within downscaling models.

Acknowledgments. This work was supported by the European Commission of the European Union under Contract ENV4-CT95-0121. Financial assistance has also been provided by the Gulbenkian Foundation (Portugal) and from the School of Environmental Sciences of the University of East Anglia (UK). R.M.T was supported by a Grant (BD/5734/95-RN) from the FCT (Portugal) under the PRAXIS Program. Model data from the Hadley Centre were supplied by David Viner through the Climate Impacts LINK Project (EPG 1/1/16). Monthly gridded precipitation and sea level pressure were kindly supplied by Mike Hulme and Phil Jones from the Climatic Research Unit.

REFERENCES

Arnell, N. W., 1999: The effect of climate change on hydrological regimes in Europe: A continental prespective. *Global. Environ. Change,* **9,** 5–23.

Barnston, A. G., and R. E. Livezey, 1987: Classification, seasonality, and persistence of low-frequency atmospheric circulation patterns. *Mon. Wea. Rev.,* **115,** 1083–1127.

Barrow, E. M., M. Hulme, and M. Semenov, 1996: The effect of using different methods in the construction of climate change scenarios: Examples from Europe. *Climate Res.,* **7,** 195–211.

Bürger, G., 1996: Expanded downscaling for generating local weather scenarios. *Climate Res.,* **7,** 111–128.

Busuioc, A., H. von Storch, and R. Schnur, 1999: Verification of GCM-generated regional seasonal precipitation for current climate and statistical downscaling estimates under changing climate conditions. *J. Climate,* **12,** 258–272.

Cavazos, T., 1997: Downscaling large-scale circulation to local winter

rainfall in north-eastern Mexico. *Int. J. Climatol.,* **17,** 1069–1082.

——, 1999: Large-scale circulation anomalies conductive to extreme precipitation events and derivation of daily rainfall in north-eastern Mexico and southeastern Texas. *J. Climate,* **12,** 1506–1523.

Christensen, J. H., B. Machenhauer, J. R. Jones, C. Schär, P. M. Ruti, M. Castro, and G. Visconti, 1997: Validation of present-day regional climate simulations over Europe: LAM simulations with observed boundary conditions. *Climate Dyn.,* **13,** 489–506.

Corte-Real, J., X. Zhang, and X. Wang, 1995: Downscaling GCM information to regional scales: A non-parametric multivariate approach. *Climate Dyn.,* **11,** 413–424.

——, B. Qian, and H. Xu, 1998: Regional climate change in Portugal: Precipitation variability associated with large-scale atmospheric circulation. *Int. J. Climatol.,* **18,** 619–635.

——, H. Xu, and B. Qian, 1999: A weather generator for obtaining daily precipitation scenarios based on circulation patterns. *Climate Res.,* **13,** 61–75.

Crane, R. G., and B. C. Hewitson, 1998: Doubled CO_2 climate change scenarios for the Susquehanna Basin: Precipitation. *Int. J. Climatol.,* **18,** 65–76.

Cubasch, U., H. von Storch, J. Wasekewitz, and E. Zorita, 1996: Estimates of climate change in southern Europe using different downscaling techniques. *Climate Res.,* **7,** 129–149.

Glowienka-Hense, R., 1990: Performance of the ECMWF T21 model in simulating the North Atlantic oscillation in the Atlantic–European SLP field. *Tellus,* **42A,** 497–507.

Gonzalez-Rouco, F., E. Zorita, H. Heyen, and F. Valero, 2000: Agreement between observed rainfall trends and climate change simulations in the southwest of Europe. *J. Climate,* **13,** 3057–3065.

Goodess, C. M., and J. P. Palutikof, 1998: Development of daily rainfall scenarios for Southeast Spain using a circulation type approach to downscaling. *Int. J. Climatol.,* **18,** 1051–1081.

——, and P. D. Jones, 2001: Links between circulation and changes in the characteristics of Iberian rainfall. *Int. J. Climatol.,* in press.

Hagan, M. T., H. B. Demuth, and M. H. Beale, 1996: *Neural Networks Design.* PWS Publishing Company, 736 pp.

Harrison, P. A., and R. E. Butterfield, 1996: Effects of climate change on Europe-wide wheat and sunflower productivity. *Climate Res.,* **7,** 225–241.

Hewitson, B. C., and R. G. Crane, 1996: Climate downscaling: Techniques and application. *Climate Res.,* **7,** 85–95.

——, and ——, 1998: Regional scale daily precipitation from downscaling of data from the Genesis and UKMO GCMs. Preprints, *14th Conf. on Probability and Statistics in the Atmospheric Sciences,* Phoenix, AZ, Amer. Meteor. Soc., J48–J50.

Hulme, M., 1992: 1951–80 global land precipitation climatology for the evaluation of general circulation models. *Climate Dyn.,* **7,** 57–72.

——, 1994: Validation of large-scale precipitation fields in general circulation models. *Global Circulation and Climate Change,* M. Desbois and F. Desalmand, Eds., NATO ASI Series, Vol. I26, Springer-Verlag, 387–407.

——, E. M. Barrow, N. W. Arnell, P. A. Harrisson, T. C. Johns, and T. E. Downing, 1999: Relative impacts of human-induced climate change and natural climate variability. *Nature,* **397,** 688–691.

Hurrell, J. W., 1995: Decadal trends in the North Atlantic oscillation: Regional temperatures and precipitation. *Science,* **269,** 676–679.

Johns, T. C., R. E. Carnell, J. F. Crossley, J. M. Gregory, J. F. B. Mitchell, C. A. Senior, S. F. B. Tett, and R. A. Wood, 1997: The second Hadley Centre coupled ocean–atmosphere GCM: Model description, spinup and validation. *Climate Dyn.,* **13,** 103–134.

Jolliffe, I. T., 1990: Principal Component Analysis: A beginner's guide—I. Introduction and application. *Weather,* **45,** 375–382.

——, 1993: Principal Component Analysis: A beginner's guide—II. Pitfalls, myths and extensions. *Weather,* **48,** 246–253.

Jones, P. D., M. Hulme, and K. R. Briffa, 1993: A comparison of Lamb circulation types with an objective classification scheme. *Int. J. Climatol.,* **13,** 655–663.

Karl, T. R., W.-C. Wang, M. E. Schlesinger, R. W. Knight, and D. Portman, 1990: A method of relating general circulation model simulated climate to the observed local climate. Part I: Seasonal statistics. *J. Climate,* **3,** 1053–1079.

Laita, M., and M. Grimalt, 1997: Vorticity and pressure anomalies in the western Mediterranean during El Niño/Southern Oscillation extremes. *Int. J. Climatol.,* **17,** 475–482.

Leggett, J., W. J. Pepper, and R. J. Stewart, 1992: Emissions scenarios for IPCC: An update. *Climate Change 1992: The Supplementary Report to the IPCC Scientific Assessment,* J. T. Houghton, B. A. Callander, and S. K. Varney, Eds., Cambridge University Press, 69–95.

North, G. R., T. L. Bell, R. F. Cahalan, and F. J. Moeng, 1982: Sampling errors in the estimation of empirical orthogonal functions. *Mon. Wea. Rev.,* **110,** 699–706.

Osborn, T. J., 1997: Areal and point precipitation intensity changes: Implications for the application of climate models. *Geophys. Res. Lett.,* **24,** 2829–2832.

——, and M. Hulme, 1998: Evaluation of the European daily precipitation characteristics from the Atmospheric Model Intercomparison Project. *Int. J. Climatol.,* **18,** 505–522.

——, K. R. Briffa, S. F. B. Tett, P. D. Jones, and R. M. Trigo, 1999: Evaluation of the North Atlantic oscillation as simulated by a climate model. *Climate Dyn.,* **15,** 685–702.

Palutikof, J. P., J. A. Winkler, C. M. Goodess, and J. A. Andresen, 1997: The simulation of daily temperature time series from GCM output. Part I: Comparison of model data with observations. *J. Climate,* **10,** 2497–2513.

——, M. D. Agnew, and S. J. Watkins, 1999: Statistical downscaling of model data. Final report of the European project: Mediterranean Desertification and Land Use (MEDALUS III), Project 3; Regional Indicators, Module 11.2, 414 pp.

Preisendorfer, R. W., 1988: *Principal Component Analysis in Meteorology and Oceanography.* Vol. 17, Developments in Atmospheric Science, Elsevier, 425 pp.

Richman, M. B., 1986: Rotation of principal components. *J. Climatol.,* **6,** 293–335.

Rocha, A., 1999: ENSO and Iberian rainfall. *Int. J. Climatol.,* **19,** 889–301.

Rodó, X., E. Baert, and F. A. Comin, 1997: Variations in seasonal rainfall in southern Europe during the present century: Relationships with the North Atlantic oscillation and the El Niño–Southern Oscillation. *Climate Dyn.,* **13,** 275–284.

Rodriguez-Puebla, C., A. H. Encinas, S. Nieto, and J. Garmendia, 1998: Spatial and temporal patterns of annual precipitation variability over the Iberian Peninsula. *Int. J. Climatol.,* **18,** 299–316.

Romero, R., J. A. Guijarro, C. Ramis, and S. Alonso, 1998: A 30-year (1864–1993) daily rainfall data base for the Spanish Mediterranean region: First exploratory study. *Int. J. Climatol.,* **18,** 541–560.

Sarle, W. S., 1994: Neural networks and statistical models. *Proc. 19th Annual SAS Users Group International Conf*., Cary, NC, SAS Institute, 1538–1550.

Semenov, M. A., and E. Barrow, 1997: Use of a stochastic weather generator in the development of climate change scenarios. *Climatic Change,* **35,** 397–413.

Serrano, A., A. J. Garcia, V. L. Mateos, M. L. Cancillo, and J. Garrido, 1999: Monthly modes of variation of precipitation over the Iberian Peninsula. *J. Climate,* **12,** 2894–2919.

Shubert, S., and A. Henderson-Sellers, 1997: A statistical model to downscale local daily temperature extremes from synoptic-scale atmospheric circulation patterns in the Australian region. *Climate Dyn.,* **13,** 223–234.

Skelly, W. C., and A. Henderson-Sellers, 1996: Grid box or grid point: What type of data do GCMs deliver to climate impact researchers. *Int. J. Climatol.,* **16,** 1–8.

Trigo, R. M., and J. P. Palutikof, 1999: Simulation of daily temperatures for climate change scenarios over Portugal: A neural network model approach. *Climate Res.,* **13,** 45–59.

——, and C. C. DaCamara, 2000: Circulation weather types and their impact on the precipitation regime in Portugal. *Int. J. Climatol.,* **20,** 1559–1581.

Ulbrich, U., M. Christoph, J. G. Pinto, and J. Corte-Real, 1999: Dependence of winter precipitation over Portugal on NAO and baroclinic wave activity. *Int. J. Climatol.,* **19,** 379–390.

van Loon, H., and J. C. Rogers, 1978: The seesaw in winter temperatures between Greenland and northern Europe. Part I: General description. *Mon. Wea. Rev.,* **106,** 296–310.

von Storch, H., 1999: On the use of ''inflation'' in statistical downscaling. *J. Climate,* **12,** 3505–3506.

——, and F. W. Zwiers, 1999: *Statistical Analysis in Climate Research.* Cambridge University Press, 484 pp.

——, E. Zorita, and U. Cubasch, 1993: Downscaling of global climate change estimates to regional scales: An application to Iberian rainfall in wintertime. *J. Climate,* **6,** 1161–1171.

Wallace, J. M., and D. S. Gutzler, 1981: Teleconnections in the geopotential height field during the Northern Hemisphere winter. *Mon. Wea. Rev.,* **109,** 784–812.

Wilby, R. L., and T. M. L. Wigley, 1997: Downscaling general circulation model output: A review of methods and limitations. *Prog. Phys. Geogr.,* **21,** 530–548.

Wilks, D. S., 1995: *Statistical Methods in the Atmospheric Sciences: An introduction.* Vol. 59, International Geophysical Series, Academic Press, 464 pp.

Zhang, X., X. L. Wang, and J. Corte-Real, 1997: On the relationships between daily circulation patterns and precipitation in Portugal. *J. Geophys. Res.,* **102,** 13 495–13 507.

Zorita, E., and H. von Storch, 1999: The analog method as a simple downscaling technique: Comparison with more complicated methods. *J. Climate,* **12,** 2474–2489.